Article

Cell Metabolism

Macrophage MerTK Promotes Liver Fibrosis in Nonalcoholic Steatohepatitis

Graphical Abstract

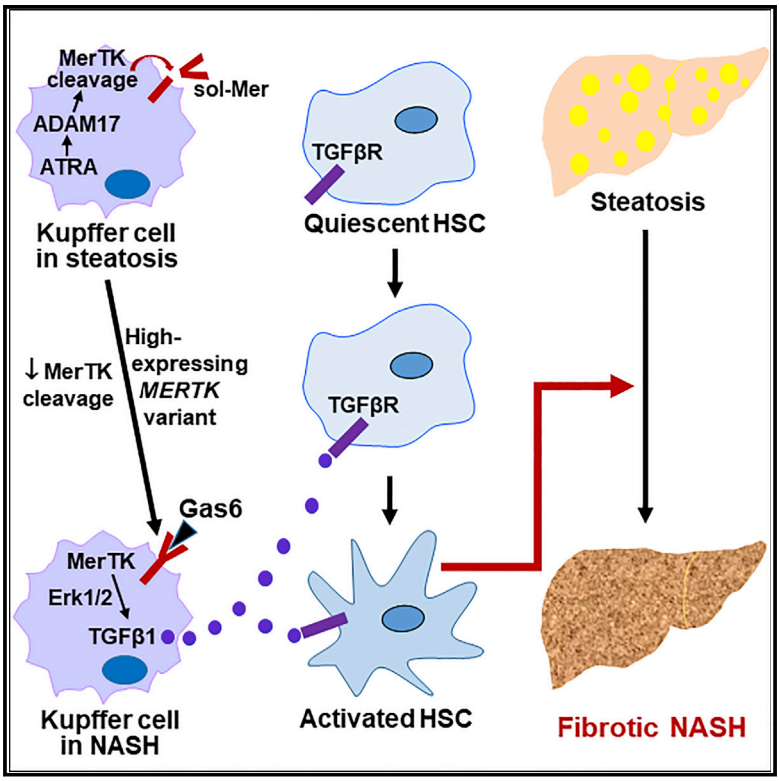

Highlights

- MerTK signaling in liver macrophages promotes liver fibrosis in NASH
- Macrophage MerTK activates hepatic stellate cells in NASH by inducing TGF-β1
- ATRA-induced MerTK cleavage blocks the TGF-b1-fibrosis pathway in steatosis
- ATRA-induced MerTK cleavage becomes defective in NASH

Authors

Bishuang Cai, Paola Dongiovanni, Kathleen E. Corey, ..., Raymond B. Birge, Luca Valenti, Ira Tabas

Correspondence

bc2586@columbia.edu (B.C.), iat1@columbia.edu (I.T.)

In Brief

Genome-wide association studies have indicated that MerTK is a risk factor for liver fibrosis in NASH with an unknown mechanism. Cai et al. discovered that MerTK signaling in liver macrophages, which is enhanced in NASH owing to suppression of its cleavage by ADAM17, promotes TGF-β1 production, HSC activation, and liver fibrosis in NASH.

Cai et al., 2020, Cell Metabolism *31*, 1–16
February 4, 2020 © 2019 Elsevier Inc.
https://doi.org/10.1016/j.cmet.2019.11.013

CellPress

Please cite this article in press as: Cai et al., Macrophage MerTK Promotes Liver Fibrosis in Nonalcoholic Steatohepatitis, Cell Metabolism (2019), https://doi.org/10.1016/j.cmet.2019.11.013

Cell Metabolism
Article

Macrophage MerTK Promotes Liver Fibrosis in Nonalcoholic Steatohepatitis

Bishuang Cai,[1,*] Paola Dongiovanni,[2] Kathleen E. Corey,[3,4] Xiaobo Wang,[1] Igor O. Shmarakov,[1] Ze Zheng,[1] Canan Kasikara,[1] Viralkumar Davra,[7] Marica Meroni,[2] Raymond T. Chung,[3,4] Carla V. Rothlin,[6] Robert F. Schwabe,[1,5] William S. Blaner,[1] Raymond B. Birge,[7] Luca Valenti,[8,9] and Ira Tabas[1,10,11,*]

[1]Department of Medicine, Columbia University Irving Medical Center, New York, NY 10032, USA
[2]General Medicine and Metabolic Diseases, Fondazione Ca' Granda IRCCS Ospedale Maggiore Policlinico, Milano 20122, Italy
[3]Liver Center, Gastrointestinal Division, Massachusetts General Hospital, Boston, MA 02114, USA
[4]Harvard Medical School, Boston, MA, USA
[5]Institute of Human Nutrition, Columbia University Irving Medical Center, New York, NY 10032, USA
[6]Department of Immunobiology, Yale University School of Medicine and Department of Pharmacology, Yale University, New Haven, CT, USA
[7]Department of Microbiology, Biochemistry and Molecular Genetics, Rutgers University, New Jersey Medical School Cancer Center, Newark, NJ 07103, USA
[8]Department of Pathophysiology and Transplantation, Università degli Studi di Milano, Milano 20122, Italy
[9]Translational Medicine – Transfusion Medicine and Hematology, Fondazione Ca' Granda IRCCS Ospedale Maggiore Policlinico, Milano 20122, Italy
[10]Departments of Pathology & Cell Biology and Physiology & Cellular Biophysics, Columbia University Irving Medical Center, New York, NY 10032, USA
[11]Lead Contact
*Correspondence: bc2586@columbia.edu (B.C.), iat1@columbia.edu (I.T.)
https://doi.org/10.1016/j.cmet.2019.11.013

SUMMARY

Nonalcoholic steatohepatitis (NASH) is emerging as a leading cause of chronic liver disease. However, therapeutic options are limited by incomplete understanding of the mechanisms of NASH fibrosis, which is mediated by activation of hepatic stellate cells (HSCs). In humans, human genetic studies have shown that hypomorphic variations in *MERTK*, encoding the macrophage c-mer tyrosine kinase (MerTK) receptor, provide protection against liver fibrosis, but the mechanisms remain unknown. We now show that holo- or myeloid-specific *Mertk* targeting in NASH mice decreases liver fibrosis, congruent with the human genetic data. Furthermore, ADAM metallopeptidase domain 17 (ADAM17)-mediated MerTK cleavage in liver macrophages decreases during steatosis to NASH transition, and mice with a cleavage-resistant MerTK mutant have increased NASH fibrosis. Macrophage MerTK promotes an ERK-TGFβ1 pathway that activates HSCs and induces liver fibrosis. These data provide insights into the role of liver macrophages in NASH fibrosis and provide a plausible mechanism underlying *MERTK* as a genetic risk factor for NASH fibrosis.

INTRODUCTION

The epidemic of obesity has led to a sharp rise in non-alcoholic liver disease (NAFLD), which can progress to nonalcoholic steatohepatitis (NASH) (Corey and Kaplan, 2014). NASH in turn can lead to the development of cirrhotic liver disease and hepatocellular carcinoma (HCC) and has emerged as the leading cause of chronic liver disease and the most rapidly growing indication for liver transplantation worldwide (Doycheva et al., 2018; Rinella, 2015; Rinella and Sanyal, 2016). Liver fibrosis is the most important predictor of long-term mortality, liver transplantation, and liver-related clinical events in NASH (Angulo et al., 2015a, 2015b; Dulai et al., 2017; Puche et al., 2013; Vilar-Gomez et al., 2018). However, there are no FDA-approved drugs to treat NASH, which is due in large part to our incomplete understanding of the mechanisms of fibrotic NASH progression.

Context and Significance

Nonalcoholic steatohepatitis (NASH) has emerged as the leading cause of chronic liver disease, with liver fibrosis being the most important predictor of liver failure. However, owing to the major gaps in understanding the mechanisms of NASH fibrosis, there are no FDA-approved drugs to treat NASH. Recent genome-wide association studies identified *MERTK* gene variations that reduce MerTK protein expression and possess protective effects against liver fibrosis in NASH, but the mechanism linking MerTK to fibrosis has remained a mystery. Using various genetic MerTK NASH mouse models and human NASH liver specimens, researchers at Columbia University show that MerTK signaling in macrophages promotes liver fibrosis, whereas blocking MerTK activation suppresses fibrosis. These data raise the possibility of unique therapeutic strategies to block NASH fibrosis.

NAFLD begins with the accumulation of large amounts of triglyceride in hepatocytes (hepatosteatosis or fatty liver), which is a relatively benign condition. However, in approximately 20% of subjects, inflammation, cell death, and fibrosis ensue, leading to NASH and then, in certain subjects, cirrhosis and HCC. Liver fibrosis in NASH and other chronic liver diseases is driven by the activation of hepatic stellate cells (HSCs), which become transformed from quiescent retinyl ester-storing cells into myofibroblasts that produce collagen and other types of extracellular matrix (Puche et al., 2013; Tsuchida and Friedman, 2017). Therefore, understanding how HSCs become activated during the progression from non-fibrotic hepatosteatosis into fibrotic NASH is a critical question in this area of research. Although many studies have uncovered pathways in which molecules secreted by liver macrophages and hepatocytes can activate HSCs, major gaps remain in our understanding of HSC activation during steatosis to NASH progression (Weiskirchen and Tacke, 2016; Tsuchida and Friedman, 2017).

Human genetics can provide important clues for treatable processes that contribute to disease pathogenesis. In a genome-wide association study (GWAS) and several independent replication cohorts, naturally occurring variations in *MERTK*, the gene that encodes c-mer tyrosine kinase (MerTK), have been identified as a contributor to the development and progression of liver fibrosis in NASH and HCV patients (Cavalli et al., 2017; Jiménez-Sousa et al., 2018; Patin et al., 2012; Petta et al., 2016). However, how MerTK may be mechanistically linked to liver fibrosis in NASH remains unknown. MerTK, which is a member of the Tyro-Axl-MerTK (TAM) family of proteins, is highly expressed on macrophages and has a number of ligands, notably Gas6 and protein S, either as free proteins or attached to apoptotic cells during MerTK-mediated clearance of apoptotic cells (efferocytosis) (Dransfield et al., 2015; Scott et al., 2001; Thorp et al., 2008). Ligand binding activates MerTK signaling pathways involved in internalization of apoptotic cells, suppression of inflammation, and synthesis of mediators of inflammation resolution and tissue repair (Cai et al., 2016, 2018; Camenisch et al., 1999; Tibrewal et al., 2008). In the aforementioned human genetic studies, two intronic single-nucleotide polymorphisms (SNPs) in *MERTK* that are in linkage disequilibrium, rs4374383 A (Patin et al., 2012; Petta et al., 2016) and rs6726639 A (Cavalli et al., 2017), were shown to be associated with lower hepatic expression of *MERTK* and a reduced risk of liver fibrosis, raising the possibility that MerTK promotes liver fibrosis. Although previous studies have suggested roles for MerTK in exacerbating pro-inflammatory monocyte activation in response to fat ingestion (Musso et al., 2017) and in Gas6 signaling in HSCs (Petta et al., 2016), no precise mechanism has been defined.

In this context, we now show that MerTK signaling in macrophages induces the expression of TGF-β1 by activating ERK1/2, and secretion of TGF-β1 by these macrophages can then activate HSCs to promote collagen synthesis. Most importantly, myeloid-specific targeting of MerTK in mice fed a high-fat NASH-promoting diet partially protects the mice from developing liver fibrosis. Interestingly, cell-surface proteolytic cleavage of MerTK, which is an ADAM metallopeptidase domain 17 (ADAM17)-mediated process that destroys MerTK signaling (Cai et al., 2016, 2017; Sather et al., 2007; Thorp et al., 2011), occurs in early, non-fibrotic steatosis but decreases with NASH progression. Moreover, NASH fibrosis is enhanced in mice expressing a cleavage-resistant (CR) mutant of MerTK. Thus, MerTK cleavage is protective in this setting. We show further that all-trans retinoic acid (ATRA), an active metabolite of retinol found in healthy liver, induces MerTK cleavage in macrophages by activating ADAM17. Finally, blocking MerTK activation in NASH mice by using a Gas6 inhibitor or by enhancing MerTK cleavage with ATRA supplementation suppressed NASH progression. These findings provide mechanistic insight related to the role of liver macrophages in NASH, suggest a plausible mechanism for the association of hypomorphic *MERTK* variants with protection against fibrosing NASH in humans, and raise the possibility of unique human genetic-based strategies to suppress NASH fibrosis.

RESULTS

Macrophage MerTK Promotes Liver Fibrosis in NASH Mice, and Macrophage MerTK Expression Is Lower in the Livers of Humans Carrying a NASH Fibrosis-Protective *MERTK* Polymorphism

Macrophages express the highest levels of MerTK among all cell types, including in liver (Gautier et al., 2012; Petta et al., 2016). To examine this point in more detail, we assayed cell-surface MerTK expression in different liver macrophage populations by flow cytometry and found that MerTK is expressed predominantly on F4/80^{hi}CD11b^{low} CLEC4F^{+} resident macrophages (Kupffer cells) (Figures S1A and S1I, gate #5). This finding is consistent with recent single-cell RNA sequencing (RNA-seq) analysis of mouse NASH liver and cirrhotic human liver, which revealed that *MERTK* is primarily expressed in liver macrophages, including Kupffer cells (Ramachandran et al., 2019; Xiong et al., 2019).To study the role of MerTK in NASH-associated liver fibrosis, we compared wild-type (WT) and *Mertk*$^{-/-}$ mice fed a NASH-promoting diet that is rich in fructose, palmitic acid, and cholesterol. After 16 weeks of feeding, this diet causes key features of NASH, including weight gain and insulin resistance; liver steatosis, inflammation, and early fibrosis; and elevated plasma alanine aminotransferase (ALT) (Wang et al., 2016). The livers from the *Mertk*$^{-/-}$ mice had undetectable MerTK but the same level of expression as WT mice of the TAM family member, Axl (Figure S1B). The two groups of mice had similar body weights, liver:body weight ratios, fasting blood glucose, plasma cholesterol, plasma triglyceride, liver cholesterol, and liver triglyceride (Figure S1C). The key finding was that liver fibrosis as assessed by Picrosirius red staining, collagen gene expression, and αSMA^{+} area was decreased in the MerTK-deficient mice (Figures 1A–1C), without a change in hepatosteatosis as assessed by lipid droplet area (Figure S1D). These data are congruent with the human genetic data, which show that loss-of-function *MERTK* variants are associated with decreased liver fibrosis in NAFLD (Petta et al., 2016). The *Mertk*$^{-/-}$ mice also had lower plasma ALT and less terminal deoxynucleotidyl transferase dUTP nick end labeling-positive (TUNEL^{+}) liver cells (Figure S1E), but inflammation-induced cytokine mRNAs, which are increased in NASH-diet-fed mice compared with chow-fed mice (Wang et al., 2016), were not different between the two cohorts (Figure S1F).

We then conducted a similar experiment to that above, but this time comparing NASH-diet-fed control (Con) *Mertk*$^{fl/fl}$ mice with *Mertk*$^{fl/fl}$*Lyz2cre*$^{+/-}$ mice, in which Cre recombinase driven

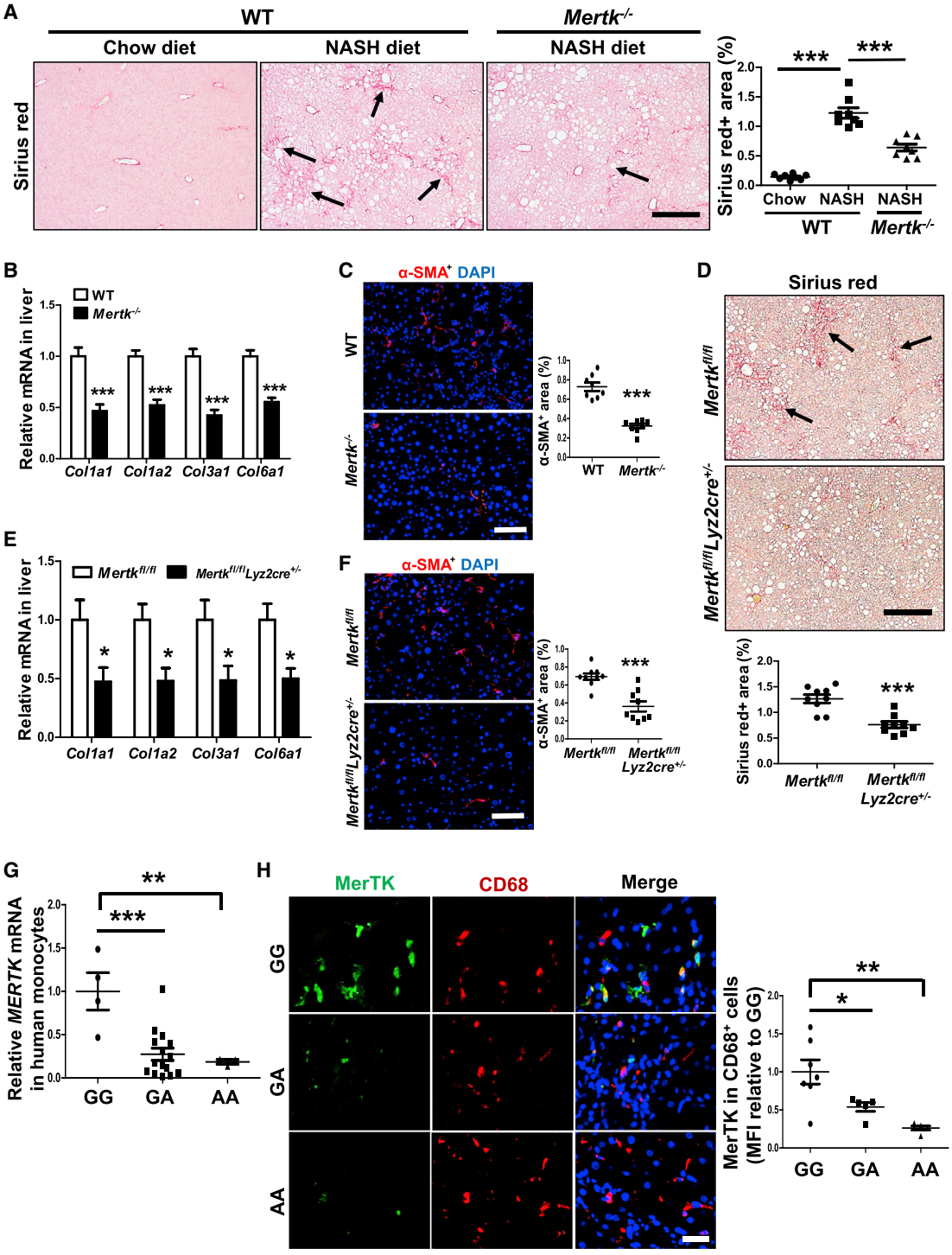

Figure 1. Macrophage MerTK Deficiency Protects against Liver Fibrosis in NASH-Diet-Fed Mice, and Humans with a NASH Fibrosis-Protective Polymorphism Have Lower MerTK Expression in Liver Macrophages

(A–C) WT or *Mertk*$^{-/-}$ male mice were fed either the chow or NASH diet for 16 weeks. (A) Liver fibrosis was detected by Picosirius red staining in liver sections and quantified as percent Picosirius red^{+} area by ImageJ; scale bar, 200 μm. (B) Liver collagen gene expression was assayed by qPCR. (C) αSMA immunofluorescence (red) and quantification; DAPI counterstain for nuclei is shown; scale bar, 200 μm. For (A)–(C), n = 8 mice per group.

(D–F) *Mertk*$^{fl/fl}$*Lyz2cre*$^{+/-}$ and littermate control *Mertk*$^{fl/fl}$ mice were fed the NASH diet for 16 weeks. Liver fibrosis, collagen gene expression, and percent αSMA^{+} area in the liver were assayed as in (A)–(C) (n = 9 mice per group); scale bar, 200 μm.

(legend continued on next page)

by the lysozyme M promoter (LysMCre) deletes floxed *Mertk* in myeloid cells (Clausen et al., 1999). *Mertk*$^{fl/fl}$*Lyz2cre*$^{+/-}$ mice and Con *Mertk*$^{fl/fl}$ mice had similar body weight, liver:body weight ratio, fasting blood glucose, plasma cholesterol, plasma triglyceride, liver cholesterol, and liver triglyceride (Figure S1G). In line with the fact that most MerTK is expressed on macrophages, whole liver extract from both chow-fed and NASH *Mertk*$^{fl/fl}$*Lyz2cre*$^{+/-}$ mice showed much less MerTK protein than liver extract from Con *Mertk*$^{fl/fl}$ mice, and F4/80^{hi}CD11b^{low} macrophages from *Mertk*$^{fl/fl}$*Lyz2cre*$^{+/-}$ mice also had much fewer MerTK^{+} cells (Figures S1H and S1I, gates 4–6). As with holo-MerTK knockout NASH mice, *Mertk*$^{fl/fl}$*Lyz2cre*$^{+/-}$ NASH mice had less liver fibrosis, collagen gene expression, αSMA^{+} area, plasma ALT, and TUNEL^{+} liver cells than *Mertk*$^{fl/fl}$ mice (Figures 1D–1F and S1J). As MerTK is an efferocytosis receptor on macrophages, we assayed efferocytosis in the livers from these mice by quantifying the ratio of macrophage-associated to free TUNEL^{+} cells and found no differences (Figure S1K). Finally, *Mertk*$^{fl/fl}$*Lyz2cre*$^{+/-}$ mice also had less liver fibrosis than *Mertk*$^{fl/fl}$ mice when the mice were fed the NASH diet for 25 weeks to increase fibrosis (Figure S1L).

As mentioned previously, NASH patients carrying the *MERTK* rs4374383 G > A variant, which is associated with reduced *MERTK* mRNA expression in the liver, have less liver fibrosis compared with those harboring the major G allele (Petta et al., 2016). In view of the above data showing that loss of myeloid MerTK suppresses NASH fibrosis, we determined whether *MERTK* mRNA was lower in blood monocytes of healthy subjects carrying the A versus G allele and, most importantly, whether MerTK expression was lower in liver macrophages of NASH patients carrying the A versus G allele. We found that subjects carrying at least one A allele had lower *MERTK* mRNA expression in blood monocytes than GG subjects (Figure 1G) and that the presence of an A allele was also associated with lower MerTK expression in liver macrophages (Figure 1H).

In summary, the mouse data show that MerTK in liver macrophages contributes to NASH progression to fibrosis, and the human data raise the possibility that the association of the A allele in rs4374383 with protection from fibrosing NASH may be due, at least in part, to its association with less MerTK expression in liver macrophages.

Activation of Macrophage MerTK Leads to an Increase in TGF-β1, which Activates HSCs to Produce Collagen

We next explored how macrophage MerTK might promote fibrosis in NASH, focusing on the concept of macrophage-HSC crosstalk. In view of the pro-fibrotic action of TGF-β in experimental NASH (Yang et al., 2014), we considered the hypothesis that MerTK activation in macrophages might increase the synthesis and secretion of TGFβ, which would then activate HSCs to promote fibrosis. As an initial test of this hypothesis, we compared *Tgfb1*, *Tgfb2*, and *Tgfb3* mRNAs in the livers of chow-fed *Mertk*$^{fl/fl}$ mice, NASH-diet-fed *Mertk*$^{fl/fl}$ mice, and NASH-diet-fed *Mertk*$^{fl/fl}$*Lyz2cre*$^{+/-}$ mice. *Tgfb1*, but not *Tgfb2* or *Tgfb3*, was markedly increased in NASH liver, and this increase was partially dependent on myeloid MerTK (Figure 2A, upper graph). TGF-β1 latency-associated peptide (LAP) expression in F4/80^{hi}CD11b^{low} liver resident macrophages was also increased in NASH liver, and it was decreased to the non-NASH liver level in mice lacking myeloid MerTK (Figure 2A, lower graph and Figure S2A). The TGF-β-fibrosis pathway driven by MerTK appears to be relatively specific, as liver expression of PDGFβ, another liver fibrosis inducer (Czochra et al., 2006), was statistically similar between the two groups of mice, and Gas6 treatment of Kupffer cells did not increase *Pdgfb* mRNA (Figure S2B).

We next isolated F4/80^{+} macrophages from the livers of WT mice (Figure S2C) to determine if MerTK activation could increase *Tgfb1* expression. The macrophages were treated with siMertk or scrambled Con siRNA (siScr) and then incubated with the MerTK activator Gas6. Consistent with the hypothesis, Gas6 treatment induced *Tgfb1* expression in liver macrophages, and this action of Gas6 was completely blocked by MerTK silencing (Figure 2B). Human monocyte-derived macrophages also showed an increase in *TGFB1* mRNA with Gas6 treatment, and this was abrogated by siMERTK (Figure 2C).

To determine whether Gas6-induced macrophage TGF-β1 can activate HSCs, conditioned media (CM) collected from Gas6-treated or Con human macrophages were treated with Con IgG or anti-TGF-β1 neutralizing IgG and then added to primary murine HSCs or HSC-T6 cells, an immortalized rat liver stellate cell line that shares many properties with primary HSCs (Vogel et al., 2000). We first analyzed TGF-β signaling in the HSC cells by immunoblotting for phospho-SMAD2/3 (p-SMAD2/3), a mediator of TGF-β signaling (Vander Ark et al., 2018). As predicted, CM from Gas6-treated macrophages increased SMAD2/3 phosphorylation, and this was suppressed by treatment of the macrophages with siMERTK or by anti-TGF-β1 treatment of the CM (Figures 2D and S2D). We then assayed *Col1a1* mRNA in the HSC cells and found exactly the same pattern: conditioned medium from Gas6-treated macrophages increased *Col1a1*, and this was prevented by silencing *MERTK* in the macrophages or by immunoneutralizing TGF-β1 in the media (Figures 2E and S2E). These *in vitro* data support the concept of a transcellular pathway leading from MerTK activation in macrophages to TGF-β1-mediated activation of HSCs. Based on previous findings, we considered the possibility that MerTK-induced TGF-β might have an additional NASH-relevant effect, namely, induction of hepatocyte death (Ciuclan et al., 2010; Tomita et al., 2012; Yang et al., 2014). Consistent with this idea and the finding of decreased cell death in livers of *Mertk*$^{-/-}$ and *Mertk*$^{fl/fl}$*Lyz2cre*$^{+/-}$ NASH mice, we found that macrophages MerTK activation induced cell death of palmitate-treated hepatocytes in a TGF-β-dependent manner (Figure S2F).

(G) Human peripheral blood monocytes were isolated from healthy subjects carrying *MERTK* rs4374383 GG, GA, or AA genotypes, and *MERTK* mRNA was assayed by qPCR (n = 22 subjects).

(H) MerTK mean fluorescence intensity (MFI) in liver CD68^{+} cells from NASH patients carrying the indicated variants at *MERTK* rs4374383 was detected by immunostaining (n = 17 subjects); scale bar, 500 μm.

Data are presented as mean ± SEM. *p < 0.05, **p < 0.01, ***p < 0.001.

See also Figure S1 and Table S1.

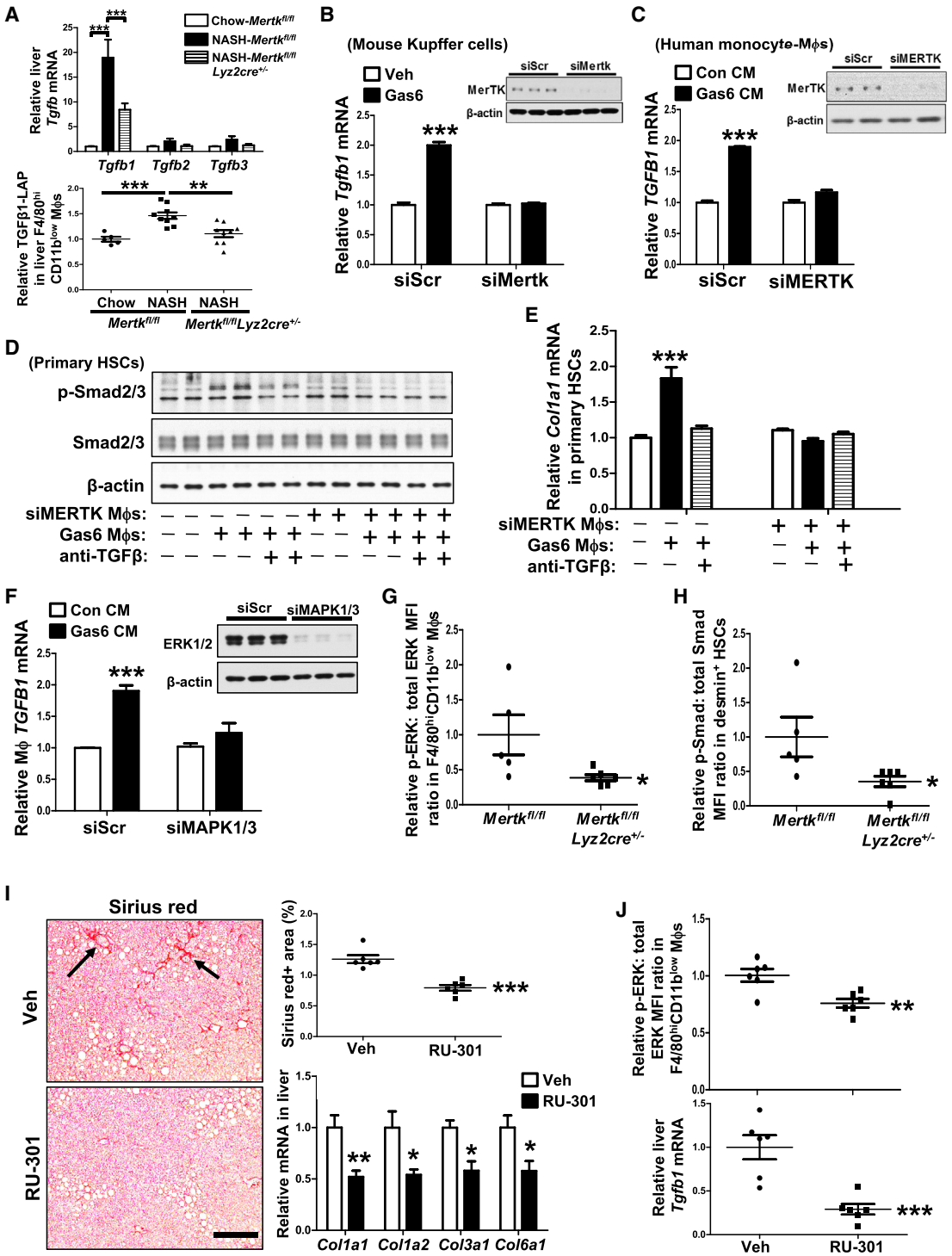

Figure 2. Activation of a MerTK-ERK-TGFβ1 Pathway in Liver Macrophages Activates HSCs and Promotes Liver Fibrosis in NASH

(A) The livers from age-matched chow-fed *Mertk*$^{fl/fl}$ mice, 16-week NASH-diet-fed *Mertk*$^{fl/fl}$ mice, and *Mertk*$^{fl/fl}$*Lyz2cre*$^{+/-}$ mice were assayed for *Tgfb1*, *Tgfb2*, and *Tgfb3* mRNA by qPCR (top graph, n = 5–9 mice per group) and TGF-β1 latency-associated peptide (LAP) on F4/80^{high}CD11b^{low} liver macrophages by flow cytometry (bottom graph, n = 5–9 mice per group).

(B) Kupffer cells were isolated from chow-fed WT mouse livers using anti-F4/80 microbeads. Kupffer cells were then treated with either scrambled siRNA (siScr) or siMertk. After 72 h, cells were treated with 100 nM purified recombinant mouse Gas6 or vehicle (Veh) for 16 h and then assayed for *Tgfb1* mRNA (n = 3 plates of macrophages per group). Inset shows MerTK immunoblot.

(C) Human monocyte-derived macrophages were treated with either siScr or siMERTK. After 72 h, the cells were treated with control (Con)- or human Gas6-conditioned media (CM) for 16 h and then assayed for *TGFB1* mRNA (n = 3 plates of macrophages per group). Inset shows MerTK immunoblot.

(legend continued on next page)

We next sought to understand how MerTK signaling in macrophages induces *TGFB1*. We reasoned that ERK1/2 may be a key signaling intermediate in this process, as it is known to be activated by MerTK (Cai et al., 2018), and the *TGFB1* transcription factor activator protein-1 (AP1) can be activated by ERK1/2 (Birchenall-Roberts et al., 1990; Liu et al., 2006; Monje et al., 2005). Consistent with this idea, Gas6-induced *TGFB1* in human macrophages was abrogated by silencing the gene encoding ERK1/2, *MAPK1/3* (Figure 2F). To show *in vivo* relevance, we used flow cytometry to assay F4/80^{hi}CD11b^{low} macrophages from the livers of *Mertk*$^{fl/fl}$ and *Mertk*$^{fl/fl}$*Lyz2cre*$^{+/-}$ NASH mice for phosphorylation of ERK, which is a measure of its activation. We found the livers from *Mertk*$^{fl/fl}$*Lyz2cre*$^{+/-}$ mice had a lower phospho-ERK:total ERK ratio (Figures 2G and S2G). Moreover, this pattern correlated with Smad phosphorylation in the HSCs from these livers (Figures 2H and S2H). These data show that ERK is an important mediator of MerTK-TGFβ1 signaling in liver macrophages.

The next goal was to learn more about the interaction of MerTK with two of its ligands, Gas6 and protein S. Analysis of liver from Con steatotic and NASH mice revealed a progressive increase in *Gas6* mRNA and Gas6 protein during NAFLD progression (Figure S2I). Although the mRNA for protein S was decreased in NAFLD versus Con liver (Figure S2J), it remained detectable in NASH liver, and, as will be shown below, protein S was able to induce *TGFB1* in human macrophages. In this context, we sought to determine the general role of MerTK ligands in the macrophage MerTK-HSC pathway in the setting of NASH. We used a compound called RU-301, which has been shown to block the functional interaction of Gas6 with TAM receptors, including MerTK (Kimani et al., 2017). We showed that RU-301 blocked the ability of Gas6 to induce *TGFB1* in human macrophages, and a similar result was obtained using an inhibitor of the tyrosine kinase activity of TAM receptors, BMS-777607 (Kasikara et al., 2017) (Figure S2K). Neither compound affected basal *TGFB1*, i.e., when macrophages were incubated in serum-free medium in the absence of MerTK ligands (Figure S2L). Protein S was also able to increase *TGFB1* in human macrophages, and although it was less potent than Gas6 at the concentration tested, protein S-induced *TGFB1* was also blocked by RU-301 (Figure S2M).

To explore *in vivo* relevance, we fed mice the NASH diet for 12 weeks and then injected the mice 3 times per week intraperitoneally (i.p.) with either DMSO or compound RU-301. After an additional 4 weeks, the livers were assayed for the macrophage MerTK-ERK-TGFβ1-fibrosis pathway. RU-301 treatment reduced liver fibrosis as indicated by decreases in liver Picrosirius red staining and collagen gene expression (Figure 2I). As predicted from the ability of RU-301 to block MerTK signaling, we further observed that the livers from RU-301-treated mice had a lower phospho-ERK:total ERK ratio, *Tgfb1* mRNA (Figure 2J), plasma ALT, and TUNEL^{+} liver cells (Figure S2N). These combined *in vitro* and *in vivo* data are consistent with a pathway in NASH in which a ligand-activated MerTK-ERK pathway in resident liver macrophages leads to the secretion of TGF-β, which can then activate HSCs and promote liver fibrosis.

Liver MerTK Cleavage Is Suppressed in NASH Fibrosis, and Mice Expressing a Genetically Engineered CR MerTK Show Increased NASH Fibrosis

The human GWAS data and the *in vitro* and *in vivo* NASH findings here support the hypothesis that MerTK signaling in liver can contribute to NASH fibrosis. In this context, we wondered whether there may be a process during the pathological progression of NASH through which liver MerTK is increased. An important mechanism that limits MerTK expression and activity in macrophages is cell-surface proteolytic cleavage by ADAM17 protease (Sather et al., 2007; Thorp et al., 2011). Moreover, the cleaved extracellular portion of the receptor—a stable protein referred to as soluble Mer (sol-Mer)—can bind Gas6 and thereby inhibit Gas6-MerTK interaction *in vitro* (Sather et al., 2007). Consistent with this idea, we found that sol-Mer prevented Gas6-induced *TGFB1* in human macrophages (Figure S3A). We therefore questioned whether there might be a decrease in MerTK cleavage in NASH fibrosis versus earlier stages of NAFLD. We studied three groups of mice; chow-fed for 16 weeks, chow-fed for 8 weeks followed by NASH-diet-fed for an additional 8 weeks, or NASH-diet-fed for 16 weeks. When mice are fed the NASH-promoting diet for 8 weeks, the liver becomes steatotic, but it does not acquire NASH features including fibrosis (Wang et al., 2016). We found that sol-Mer was markedly lower in the livers of mice fed the NASH diet for 16 weeks compared with those fed for 8 weeks (Figure 3A, top

(D and E) Human macrophages were treated as in (C). Media was removed and then the cells were rinsed and incubated in serum-free medium for 24 h. The media was collected and added to primary mouse HSCs in the presence of either 10 μg/mL anti-TGF-β1 neutralization antibody or Con IgG. One set of the HSCs was incubated with these CM for 1 h and immunoblotted for p-Smad2/3, total Smad2/3, and β-actin (D), and another set was incubated for 16 h and assayed for *Col1a1* mRNA (E) (n = 3 plates of HSCs for each condition). The CM notation below the immunoblot and graph is as follows: for siMERTK, − and + refer to siScr and siMERTK treatment, respectively; and for Gas6, − and + refer to control and Gas6 treatment, respectively.

(F) Human macrophages were treated with either siScr or siMAPK1/3. After 72 h, the cells were incubated with Con- or Gas6-CM for 16 h, followed by assay of *TGFB1* mRNA (n = 4 plates of cells). Inset shows ERK1/2 immunoblot.

(G) *Mertk*$^{fl/fl}$*Lyz2cre*$^{+/-}$ and Con *Mertk*$^{fl/fl}$ mice were fed the NASH diet for 16 weeks. Liver cells were isolated and stained with anti-CD45, F4/80, CD11b, phospho-ERK (p-ERK), or ERK antibodies, and p-ERK and ERK MFI in F4/80^{high}CD11b^{low} macrophages were analyzed by flow cytometry and expressed as p-ERK:total ERK MFI ratio.

(H) As in (G), but here the cells were stained with anti-p-Smad2/3, Smad2/3, and desmin antibodies, and the data are expressed as p-Smad2/3:total Smad2/3 MFI ratio in desmin^{+} HSCs. For (G) and (H), n = 5–6 mice per group.

(I) WT mice were fed the NASH diet for 12 weeks and then injected i.p. with 300 mg/kg body weight of RU-301 or vehicle Con 3× per week for an additional 4 weeks. Livers were assayed for Picosirius red^{+} area and collagen gene expression (n = 6 mice per group). Scale bar, 200 μM.

(J) F4/80^{high}CD11b^{low} liver macrophages (top) and liver extracts (bottom) from the mice in (I) were assayed for p-ERK:total ERK MFI ratio by flow cytometry and liver *Tgfb1* mRNA by qPCR, respectively (n = 6 mice per group).

Data are presented as mean ± SEM. *p < 0.05, **p < 0.01, ***p < 0.001.

See also Figure S2 and Table S1.

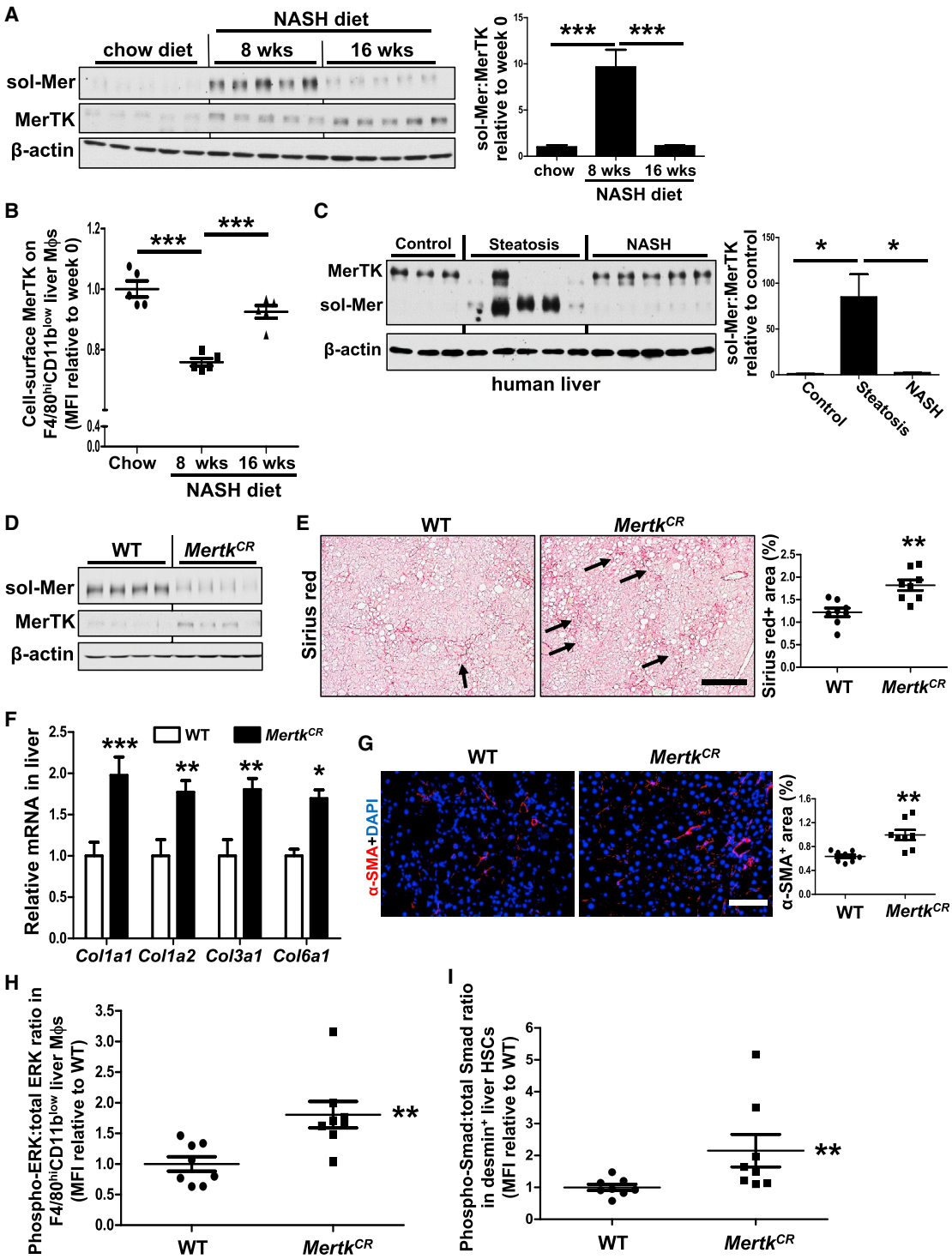

Figure 3. MerTK Cleavage Is Suppressed in Fibrotic versus Steatotic Liver in NASH-Diet-Fed Mice, and Nash-Induced Liver Fibrosis Is Enhanced in MerTK Cleavage-Resistant Mice

(A) Mice were fed the chow diet for 16 weeks, chow diet for 8 weeks and then NASH diet for an additional 8 weeks, or NASH diet for 16 weeks. Liver sol-Mer, MerTK, and β-actin were assayed by immunoblot. The ratio of sol-Mer to MerTK was quantified by Image J (n = 5 mice per group).

(B) Liver cells from the mice in (A) were isolated and stained with anti-MerTK, CD45, F4/80, and CD11b antibodies. Surface MerTK on F4/80^{high} CD11b^{low} macrophages was assayed by flow cytometry (n = 5 mice per group).

(C) MerTK and sol-Mer were assayed by immunoblot in extracts of control, steatotic, and NASH human livers. Pathology data are shown in Table S2. The ratio of sol-Mer to MerTK was quantified by ImageJ (n = 3–5 subjects per group).

(legend continued on next page)

blot). Conversely, intact MerTK was higher in the mice fed the diet for 16 weeks compared with 8 weeks without a change in *Mertk* mRNA (Figure S3B), and thus the ratio of sol-Mer to intact MerTK was markedly lower in these NASH mice (Figure 3A, middle blot and graph). We next examined F4/80^{hi}CD11b^{low} resident macrophages from these livers for cell-surface MerTK by flow cytometry. Macrophages from mice fed the NASH diet for 16 weeks had a higher expression of cell-surface MerTK than those from mice fed the diet for 8 weeks (Figure 3B). Recruited F4/80^{low}CD11b^{hi} macrophages from these livers had a relatively low level of cell-surface MerTK relative to resident F4/80^{hi}CD11b^{low} macrophages from normal livers (Figure S3C). To link these findings to human NAFLD, we were able to obtain a few samples of Con, steatotic, and NASH liver from humans for immunoblotting. As with the mouse study, the sol-Mer:intact MerTK ratio was much higher in steatotic liver than in NASH liver (Figures 3C and S3D). We also had access to liver sections from another cohort of normal, steatotic, and fibrotic NASH human liver that were available for immunostaining for MerTK and CD68$^+$ macrophages. We found that macrophage MerTK staining was lowest in steatotic liver and highest in NASH liver (Figure S3E). These combined data support the idea that MerTK cleavage is decreased in NASH versus steatotic liver, which contributes to higher cell-surface MerTK in NASH.

The above data, when considered together with the previous data herein and the human genetic studies, suggest that (1) macrophage MerTK cleavage in hepatosteatosis protects against fibrosis, i.e., by decreasing pro-fibrotic MerTK signaling to HSCs, and (2) decreased MerTK cleavage during NASH progression contributes to loss of this protection. To test this idea, we studied mice whose endogenous *Mertk* gene has been replaced with a mutant *Mertk* encoding a CR but fully functional MerTK receptor (*Mertk*^{CR} mice) (Cai et al., 2016, 2017). After 8 weeks of NASH diet feeding, which is a time of high MerTK cleavage in WT mice, sol-Mer was markedly decreased in *Mertk*^{CR} mice and vice versa for intact MerTK (Figure 3D), indicating low cleavage. After being fed the NASH diet for 16 weeks, *Mertk*^{CR} mice and WT mice had similar body weights, liver:body weight ratios, fasting blood glucose, plasma cholesterol, plasma triglyceride, liver cholesterol, liver triglyceride, liver lipid droplet area, and liver inflammatory gene mRNAs (Figures S3F–S3H). Most importantly, the livers of *Mertk*^{CR} mice showed an increase in NASH fibrosis (Figure 3E), and this was accompanied by increases in collagen gene expression, αSMA$^+$ area, TUNEL$^+$ liver cells, and plasma ALT (Figures 3F, 3G, and S3I). We next assayed *Tgfb1* mRNA in the livers of WT and *Mertk*^{CR} mice on the chow or NASH diet for 8 or 16 weeks (Figure S3J). Eight weeks of NASH diet caused an increase in *Tgfb1* in both groups, consistent with the increase in Gas6 at this time point, and it was higher in CR versus WT, consistent with increased MerTK signaling in CR macrophages. *Tgfb1* increased further by 16 weeks, concomitant with the further rise in Gas6 between 8 and 16 weeks, but the difference between WT and CR at 16 weeks was not as great as that seen at 8 weeks, as MerTK cleavage in liver macrophages in WT mice is suppressed at this time point. Macrophage ERK activation and HSC Smad activation were also increased in the livers of *Mertk*^{CR} mice versus WT mice (Figures 3H and 3I), indicating activation of the signaling pathways described previously. Thus, as predicted from the *in vitro* data, MerTK cleavage during NAFLD limits NASH fibrosis.

ATRA Induces MerTK Cleavage via a P38-ADAM17 Pathway in Macrophages

Having established the importance of MerTK cleavage as an initially protective mechanism in NAFLD mice, we next sought to determine processes that could contribute to the regulation of MerTK cleavage in NAFLD. As MerTK is cleaved by ADAM17 Sather et al., 2007; Thorp et al., 2011, we examined ADAM17 activity in liver extracts from the chow- and NASH-diet-fed mice in the previous section. ADAM17 activity was higher in the livers of the 8-week NASH-diet-fed mice (steatosis) compared with the livers of the 16-week-fed mice (NASH) (Figure 4A), which is consistent with the pattern of MerTK cleavage. ADAM17 protein was not higher in 8- versus 16-week-fed mice (Figure S4A, top blot), suggesting that ADAM17 enzymatic activity was higher in the steatotic versus NASH livers. Furthermore, as previously reported, F4/80$^+$ liver macrophages were more numerous in 16- versus 8-week-fed mice (Wang et al., 2016) (Figure S4A, 2nd blot), suggesting that ADAM17 activity per liver macrophages was markedly higher in steatotic versus NASH livers.

To investigate what might contribute to the higher ADAM17 activity in a steatotic liver, we turned to *in vitro* experiments using mouse bone-marrow-derived macrophages (BMDMs). We conceived a hypothesis based on the following previous findings in the literature: (1) P38 can activate ADAM17 (Killock and Ivetić, 2010; Thorp et al., 2011; Xu and Derynck, 2010; Xu et al., 2012) and thereby induce MerTK cleavage (Sather et al., 2007), (2) the active retinol metabolite ATRA can activate P38 in various cell types (Alsayed et al., 2001; Dai et al., 2004; Liu et al., 2014; Ren et al., 2007), (3) liver retinol is lower in the livers of subjects with NASH compared with subjects with simple steatosis (Chaves et al., 2014) and in the livers of cirrhotic patients compared with healthy controls (Ukleja et al., 2002), and (4) serum ATRA concentrations were reported to be lower in NASH patients versus Con subjects (Liu et al., 2015). We thus hypothesized that a decrease in ATRA during NASH progression might lower an important signal for the P38-ADAM17-MerTK cleavage pathway (Sather et al., 2007), leading to less MerTK cleavage in NASH.

To investigate this hypothesis, we assayed ADAM17 in BMDMs before and after treatment with ATRA. ADAM17 activity increased after 30 min of ATRA treatment and remained elevated

(D–I) WT and *Mertk*^{CR} mice were fed the NASH diet for either 8 weeks (D) or 16 weeks (E–I). (D and E) Liver extracts were assayed for sol-Mer, MerTK, and β-actin by immunoblot; scale bar, 200 μM. Liver fibrosis was detected by Picosirius red staining and quantified as % Picosirius red$^+$ area by ImageJ. (F) Liver collagen gene expression was detected by qPCR. (G) αSMA immunofluorescence (red) and quantification; DAPI counterstain for nuclei is shown; scale bar, 200 μm. (H and I) Liver macrophages and HSCs were assayed for p-ERK:total ERK MFI ratio or p-Smad2/3:total Smad2/3 MFI ratio, respectively, by flow cytometry. For (D)–(I), n = 8 mice per group.

Data are presented as mean ± SEM. *p < 0.05, **p < 0.01, ***p < 0.001.

See also Figure S3 and Tables S1 and S2.

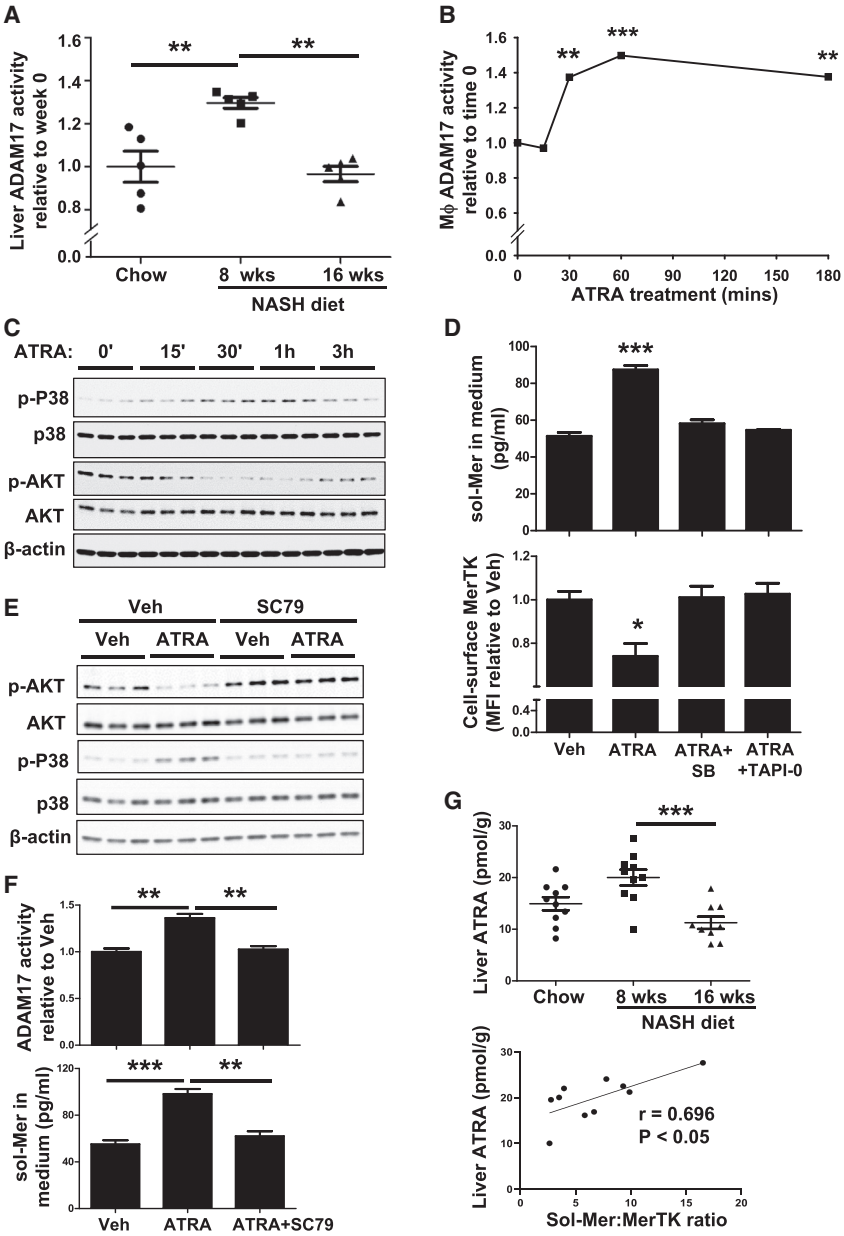

Figure 4. ATRA Induces MerTK Cleavage via a P38-ADAM17 Pathway in Macrophages

(A) WT mice were fed the chow diet for 16 weeks, chow diet for 8 weeks and then NASH diet for an additional 8 weeks, or NASH diet for 16 weeks. Liver ADAM17 activity was assayed and normalized to liver ADAM17 protein (n = 5 mice per group).

(B and C) Mouse bone-marrow-derived macrophages (BMDMs) were incubated in Dulbecco's Modified Eagle Media (DMEM) media containing 3% fetal bovine serum (FBS) for 4 h and then treated with 10 μM ATRA for the indicated times. ADAM17 activity was assayed at the indicated time points, and cell lysates were immunoblotted for p-P38, P38, p-AKT, and AKT. For (B), n = 4 plates of macrophages per time point.

(D) BMDMs (~10^6 cells) were treated with ATRA for 3 h in the absence or presence of 10 μM P38 inhibitor (SB203580) or 10 μM ADAM17 inhibitor (TAPI-0). Sol-Mer in the culture medium was detected by ELISA, and cell-surface MerTK was assayed by flow cytometry (n = 3 plates of macrophages per condition).

(E and F) BMDMs were incubated in DMEM media containing 3% FBS for 4 h, pre-treated with 5 μM SC79 for 10 min, and then incubated with 10 μM ATRA for 1 h. Cell lysates were assayed for p-P38, P38, p-AKT, and AKT by immunoblot and for ADAM17 activity. A parallel set of cells was incubated with ATRA for 3 h, and the culture media was assayed for sol-Mer (n = 3 plates of macrophages per condition).

(G) Mice were treated as in (A), and livers were assayed for ATRA by liquid chromatography-tandem mass spectrometry (LC-MS/MS) (upper graph, n = 9–10 mice per group) and for sol-Mer:MerTK ratio by immunoblot as in Figure 3A. The correlation between liver ATRA and MerTK cleavage was determined by linear regression, with the *r* and p values indicated. Data are presented as mean ± SEM. *p < 0.05, **p < 0.01, ***p < 0.001.

See also Figure S4.

for the next 2.5 h (Figure 4B), whereas ADAM17 protein was not increased by ATRA (Figure S4B). We then followed P38 activation by assaying phospho-P38 by immunoblot and found that ATRA increased the phospho-P38:total P38 ratio, which was most evident at the 30- and 60-min time points (Figure 4C). Most importantly, ATRA was able to induce MerTK cleavage in these macrophages, as shown by an increase in sol-Mer and a decrease in cell-surface MerTK, and this ATRA-induced cleavage was blocked by both a P38 inhibitor and an ADAM17 inhibitor (Figure 4D). ATRA has been shown to activate P38 by downregulating protein kinase B (AKT) activity (Gianni et al., 2002). In this context, we found that ATRA-induced P38 activation in BMDMs was associated with a decrease in the ratio of phospho-AKT:total AKT, indicating reduced AKT activation, and the AKT activator SC79 (Jo et al., 2012) blocked ATRA-induced P38 and ADAM17 activation and MerTK cleavage (Figures 4E and 4F). Similar to the findings with BMDMs, ATRA suppressed phospho-AKT (p-AKT) and increased phospho-P38 (p-P38), ADAM17 activity, and MerTK cleavage in isolated Kupffer cells (Figures S4C and S4D). ATRA-induced MerTK cleavage did not require retinoic acid receptors (RARs), as neither *Rara* and *Rarb* siRNAs nor the pan-RAR antagonist AGN 193109 (Levi et al., 2015) decreased ATRA-induced MerTK cleavage, despite good silencing efficacy of the siRNAs (Figures S4E–S4G) and demonstration that both treatments lowered a known ATRA-induced mRNA, *Arg1* (Chang et al., 2013) (Figures S4G and S4H). We then returned to our *in vivo* model by analyzing mice fed the chow or NASH diet for 8 or 16 weeks. Consistent with our hypothesis, ATRA was lower in NASH liver versus steatotic liver (Figure 4G, top). Moreover, we took advantage of the mouse-to-mouse variation in both liver ATRA and MerTK cleavage in the 8-week steatosis cohort to test correlation. When these two parameters were plotted

against each other, there was a strong positive correlation (Figure 4G, bottom). In summary, ATRA can induce MerTK cleavage in macrophages via an AKT-P38-ADAM17 pathway, and the decreases in ADAM17 activity and MerTK cleavage that are seen in NASH versus steatotic liver correlate with a decrease in liver ATRA. These data suggest that the decrease in retinoic acid that occurs during steatosis to NASH progression may be one factor that suppresses ADAM17-mediated MerTK cleavage.

Treatment of Mice with ATRA during Steatosis-to-NASH Progression Maintains MerTK Cleavage and Suppresses Fibrosis in WT but Not *Mertk*^{CR} Mice

To investigate causation among liver ATRA, MerTK cleavage, and fibrosis, we "restored" ATRA in NASH mice by treating them with a relatively low dose of ATRA (15 μg/g body weight i.p.) between weeks 8 and 16 of NASH diet feeding, i.e., the time period during which liver ATRA levels drop. As ATRA can have multiple effects in the liver, we compared WT mice with *Mertk*^{CR} mice to determine whether any observed effects of ATRA on fibrosis were dependent on MerTK cleavage. ATRA treatment caused slight but statistically significant decreases in body weight and liver:body weight ratio in both WT and *Mertk*^{CR} mice, while fasting blood glucose and liver inflammatory gene mRNAs were unaffected (Figures S5A and S5B). As designed, the mice treated with ATRA had higher but not excessive levels of ATRA in the liver (Figure S5C), with the concentration being similar to that in the steatotic liver in Figure 4G. Consistent with the hypothesis and *in vitro* data, ATRA administration caused an increase in sol-Mer and a reciprocal decrease in intact MerTK in the livers of WT but not *Mertk*^{CR} mice (Figure 5A). ATRA also caused an increase in liver phospho-P38 and ADAM17 activity, and in line with the proposed pathway in which these parameters are upstream of MerTK cleavage, these results were similar in WT and *Mertk*^{CR} mice (Figures 5B and 5C).

Analysis of the livers for Picosirius red staining and collagen gene expression in the two vehicle (Veh)-treated groups showed, as before, that fibrosis was increased in the *Mertk*^{CR} cohort (Figures 5D and 5E, Veh-WT versus Veh-Mertk^{CR}). Moreover, consistent with a previous report (Kim et al., 2014), ATRA ameliorated steatosis in the livers of WT mice, but this appeared to be unrelated to MerTK cleavage, as ATRA treatment also lowered steatosis in *Mertk*^{CR} mice (Figures 5D and S5D, Veh versus ATRA groups). Most importantly, ATRA treatment lowered liver fibrosis, collagen gene expression, and αSMA^{+} area in WT mice but not in *Mertk*^{CR} mice (Figures 5D–5F). The same pattern was seen with plasma ALT and the percentage of TUNEL^{+} liver cells (Figure S5E). Thus, treatment of mice with ATRA during the period of steatosis-to-NASH progression appears to have two distinct effects on the liver: reversal of steatosis and suppression of fibrosis. The steatosis-reversal effect is independent of MerTK cleavage, with previous reports suggesting various other mechanisms (Berry and Noy, 2009; Kim et al., 2014). In contrast, the anti-fibrotic effect is dependent on MerTK cleavage, which is consistent with our data showing links between macrophage MerTK signaling and liver fibrosis in NASH and between ATRA and MerTK cleavage in macrophages.

DISCUSSION

The primary finding in this study is the discovery of a liver macrophage-HSC crosstalk pathway in steatosis-to-NASH fibrosis progression that is triggered by activation of the MerTK receptor on resident liver macrophages and regulated by MerTK cleavage (Figure S5F). We provide correlative evidence for this pathway in humans, and the association of certain *MERTK* polymorphisms in humans with low MerTK expression and relative protection from fibrotic NASH provides further support for the role of MerTK in liver fibrosis in humans. One of the more interesting issues raised by this work is how repair and resolution pathways, particularly as orchestrated by various macrophage phenotypes, can become maladaptive in certain disease settings, including fibrotic liver disease (Gieseck et al., 2018; Hart et al., 2017). Macrophage MerTK signaling and MerTK-mediated efferocytosis participate in repair and resolution, e.g., in the setting of atherosclerosis and myocardial infarction (Cai et al., 2016, 2017; DeBerge et al., 2017). For example, MerTK pro-resolving signaling in atherosclerotic lesional macrophages stabilizes atherosclerotic plaques, in part by increasing the thickness of the collagenous fibrous cap, and MerTK cleavage during plaque progression contributes to the formation of unstable, thin-capped atheroma (Cai et al., 2017). The findings in the current study suggest that in the setting of NAFLD, the macrophage MerTK-mediated pro-fibrotic response becomes maladaptive, and thus genetic polymorphisms that lower MerTK or processes that promote MerTK cleavage are protective in this particular setting. This concept raises the issue as to whether the loss of the beneficial roles of MerTK in humans possessing loss-of-function variants or in steatosis as a result of MerTK cleavage may have some detrimental consequences in NAFLD. However, there are other mechanisms of resolution in the setting of NAFLD (Spite, 2019), and at the time that liver cell death increases in NASH (Schwabe and Luedde, 2018), cell-surface MerTK is restored owing to less cleavage.

The mechanism of how macrophage MerTK increases hepatic fibrosis in NASH in a manner consistent with the human *MERTK* genetic data represents an unexplored area of investigation. Interestingly, mouse models of liver injury that are not related to NASH or that are too far separated from human NASH may not capture the directionality of the human genetic data for NASH (Bellan et al., 2019), where variants that lower MerTK expression are associated with protection against NASH fibrosis (Petta et al., 2016). For example, liver injury in mice was exacerbated by holo-MerTK deficiency in mice given hepatotoxic amounts of acetaminophen or subjected to a choline-deficient high-fat diet for 8 weeks (Triantafyllou et al., 2018; Tutusaus et al., 2019). Future studies will be needed to investigate the mechanisms of the differences in MerTK effects between these two models and both the human genetic directionality in NASH and the NASH model used here, which uses a NASH-promoting diet without other manipulations (Wang et al., 2016). One possibility is that the anti-inflammatory and pro-resolving properties of macrophage MerTK signaling may predominate in these other models of liver injury, whereas the maladaptive, pro-fibrotic response is the major effect of MerTK signaling in human and mouse NASH models that capture certain key features of human NASH. With regard to other studies related to TAM receptors in

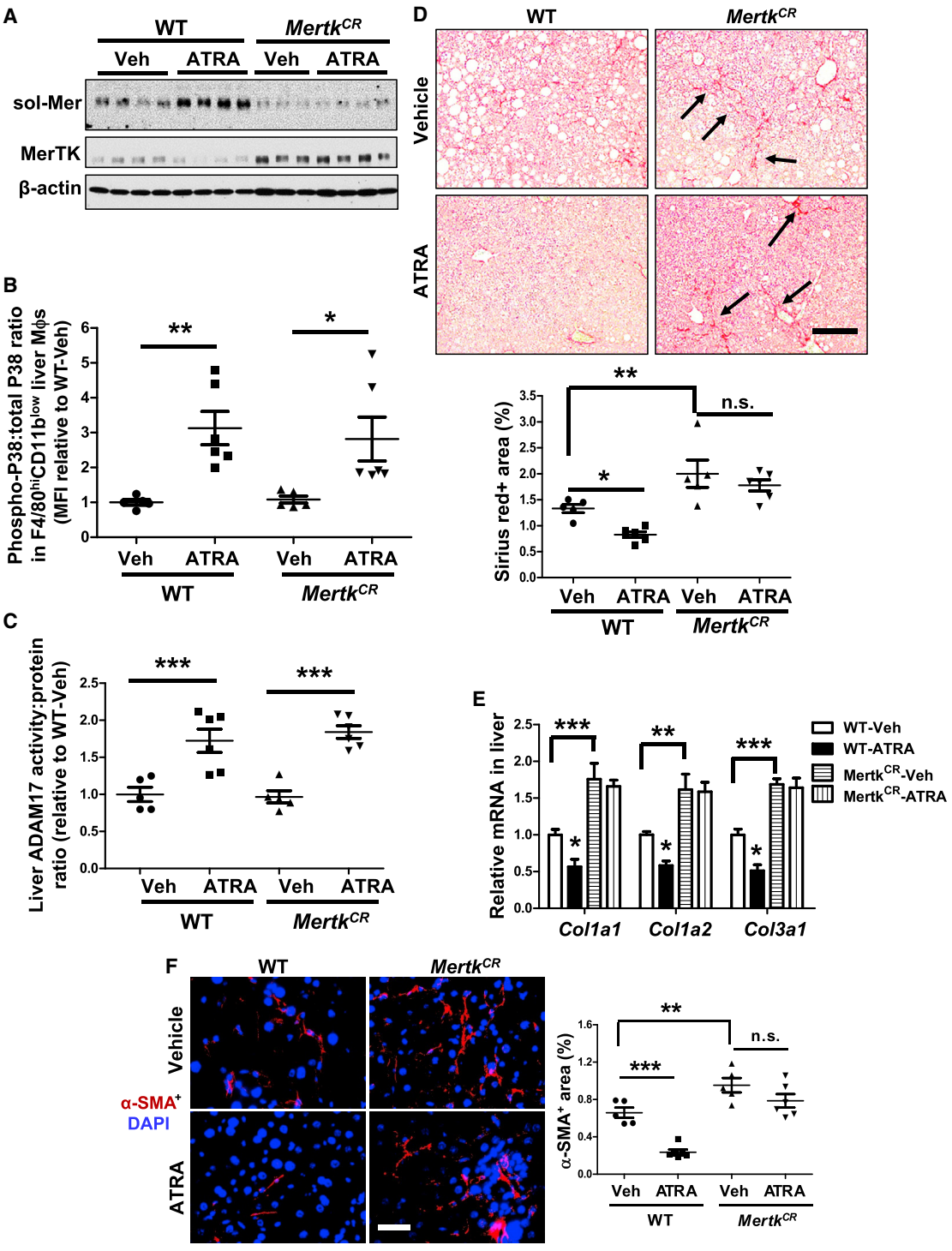

Figure 5. ATRA Induces MerTK Cleavage and Reduces Liver Fibrosis in WT but Not in *Mertk*^{CR} NASH Mice

(A–F) WT and *Mertk*^{CR} mice were fed the NASH diet for 16 weeks. During the last 8 weeks, the mice were injected i.p. with 15 μg/g body weight of ATRA or vehicle control three times a week. (A) Liver sol-Mer, MerTK, and β-actin were detected by immunoblot. (B and C) 16 h after the last of ATRA injection, the p-P38:P38 ratio in liver macrophages was determined by flow cytometry, and liver ADAM17 activity was assayed and normalized to liver ADAM17 protein (n = 5–6 mice per group). (D and E) Liver fibrosis and collagen gene expression were assayed by Picosirius red staining and qPCR, respectively; scale bar, 200 μm. (F) αSMA immunofluorescence (red) and quantification; DAPI counterstain for nuclei is shown; scale bar, 500 μm. For (D)–(F), n = 5–6 mice per group.

Data are presented as mean ± SEM. *p < 0.05, **p < 0.01, ***p < 0.001.

See also Figure S5 and Table S1.

liver disease, Gas6 can be secreted from either HSCs (Bárcena et al., 2015; Lafdil et al., 2006) or macrophages (Nepal et al., 2019) and is increased in NASH, suggesting a mechanism that could trigger macrophage MerTK signaling in NASH. In this context, holo-knockout of Gas6 in a model of steatohepatitis has been shown to lessen liver inflammation and fibrosis, although in this study there was no link to TAM receptors per se (Fourcot et al., 2011). Other studies have examined how holo-absence of Axl affects various types of liver disease, with the understanding that Axl and MerTK have different functions. For example, *Axl*$^{-/-}$ mice exposed to CCl_4 or fed the aforementioned choline-deficient high-fat diet were shown to have less HSC activation and less fibrosis (Bárcena et al., 2015; Tutusaus et al., 2019). However, the cell-specific effects of MerTK and Axl are not yet known. Thus, much remains to be learned about the role of TAM receptors in various forms of liver injury, but the data herein, in concert with the human GWAS data, strongly support a pro-fibrotic role of macrophage MerTK in NASH.

A major theme of the study is macrophage-HSC crosstalk in liver fibrosis. In that context, liver macrophages can promote fibrosis in liver disease by a number of mechanisms in addition to the one reported here. For example, IL-1 and TNF secreted by inflammatory liver macrophages triggers an NF-κB survival pathway in HSCs *in vitro* and contributes to HSC activation and liver fibrosis in bile-duct-ligated and CCl_4-treated mice (Pradere et al., 2013). In other settings, such as recovery from liver injury, liver macrophages can limit hepatic fibrosis by secreting matrix metalloproteinases (MMPs) (Duffield et al., 2005; Fallowfield et al., 2007). Whereas the macrophage MerTK pathway revealed here is clearly distinct from the inflammatory macrophage pathway that promotes HSC survival, it remains possible that MerTK-induced suppression of MMP activity is an additional fibrosis-promoting mechanism, as inhibition of MerTK in lipopolysaccharide-treated macrophages increases MMP activity (Lee et al., 2012).

Although the major mechanism of MerTK increase during steatosis-to-NASH progression in mice is decreased MerTK cleavage, with evidence of this occurring in human NASH, the mechanism of decreased MerTK in subjects harboring the lower-risk polymorphisms is not known. Transcriptional rather than post-translational regulation is likely, which is consistent with our data showing that the presence of the protective A allele at rs4374383 is associated with lower expression of *MERTK* mRNA in blood monocytes. In this context, the rs4374383 site is at an active intronic enhancer region in various cells, including human blood monocytes, according to the Encyclopedia of DNA Elements (ENCODE) and Roadmap Epigenomics Consortium databases. Moreover, the lower-*MERTK*, fibrosis-protective minor allele of rs4374383 is in linkage disequilibrium with another lower-*MERTK*, protective minor allele, rs6726639, which shows increased binding of transcriptional repressors, notably IRF1 (Cavalli et al., 2017). Regardless of mechanism *MERTK* transcriptional regulation, we propose that in subjects progressing from steatosis to NASH, lower *MERTK* expression resulting from low-risk polymorphisms may partially mitigate the effect of increased cell-surface MerTK resulting from suppressed receptor cleavage. It must be noted, however, that while our findings provide a plausible mechanism for the human genetic findings, additional mechanisms could be involved either at the *MERTK* locus itself or at possible distant loci that are regulated by polymorphisms at the *MERTK* locus.

Our investigation as to why MerTK cleavage is higher in steatotic liver versus NASH liver led to the discovery of ATRA as an activator of ADAM17 and MerTK cleavage in macrophages. MerTK cleavage is carried out by endogenous, intracellular ADAM17 in macrophages (Thorp et al., 2011), and we have provided a plausible mechanism whereby ATRA, by activating P38 in macrophages, activates ADAM17. It is interesting to consider that retinoic acid comes from retinol that is released from HSCs when they become activated, and thus retinoic acid-induced cleavage of MerTK in liver macrophages may represent a feedback loop to Con fibrogenesis in the initial stages of liver injury. We further suggest that when there is persistent liver damage and the liver becomes depleted of retinol due to transdifferentiation of the majority of HSCs, MerTK becomes chronically activated because of suppressed cleavage, thereby driving fibrogenesis. It is also interesting to note that ATRA has been reported to directly suppress HSC activation in non-NASH settings through completely different mechanisms that involve RAR activation in HSCs, which is distinct from the RAR-independent macrophage-HSC crosstalk mechanism revealed here. ATRA has been shown to suppress HSC NF-κB and P38 activation in mouse models of liver injury induced by CCl_4 and bile duct ligation (BDL) (He et al., 2011; Hisamori et al., 2008). However, our finding that ATRA does not improve NASH when MerTK cleavage is disabled, i.e., in *Mertk*^{CR} mice, indicates that in the HSC-mediated protective actions of ATRA are not dominant in the NASH model used in this study. Finally, although we have identified ATRA as an important MerTK cleavage inducer, our previous study showed that TLR4 activation can also induce ADAM17 activation (Thorp et al., 2011). Therefore, in addition to ATRA, other factors that activate TLR4 in NASH may also contribute to ADAM17 activation and MerTK cleavage.

In summary, the data in this report have revealed a pathway in the progression from steatosis to NASH fibrosis that involves crosstalk between resident liver macrophages, which secrete TGF-β1 in response to MerTK signaling, and HSCs. In view of the importance of hepatic fibrosis in the clinical course of NASH, a future goal will be to determine how the macrophage MerTK-TGF-β1 pathway revealed here might be integrated with other pathways leading to HSC activation in NASH, including those involving inflammation, cell death, and pathways involving members of the hedgehog family that are secreted by hepatocytes and activate HSCs (Machado and Diehl, 2016; Tsuchida and Friedman, 2017; Wang et al., 2016). Finally, as there are no FDA-approved drugs for NASH despite its very high prevalence, it is interesting to imagine how these findings might identify a unique therapeutic strategy in NASH. As shown here, both RU-301, which blocks the activation of MerTK by its ligands, and ATRA, which induces MerTK cleavage and has been tested in clinical trials to prevent HCC recurrence (Baselli and Valenti, 2019; Pingitore et al., 2016; Romeo and Valenti, 2016), decrease liver fibrosis during steatosis-to-NASH progression. However, as MerTK is critical for maintaining tissue homeostasis in other settings, notably atherosclerosis (Cai et al., 2017), a strategy of blocking the MerTK pathway specifically in liver macrophages, e.g., via nanotechnology (Bartneck et al., 2014;

Giannitrapani et al., 2014), would be a key consideration in conceiving such a strategy.

Limitations of Study

Our study reveals that MerTK in Kupffer cells triggers a pro-fibrotic response during NASH progression. However, what remains unknown is whether macrophage MerTK in NASH livers participate in macrophage functions traditionally ascribed to this receptor, namely, efferocytosis, dampening of inflammation, and resolution of inflammation. Moreover, some studies have shown that Kupffer cells are protective in non-NASH liver injury models, including BDL and LPS-induced acute injury (Osawa et al., 2010; Zheng et al., 2017). Therefore, if Kupffer MerTK plays different roles in diverse injury settings, the mechanisms of these differences need to be investigated. In addition, previous studies have shown that ATRA can directly suppress HSC activation and liver fibrosis in CCl_4- and BDL-induced liver injury (He et al., 2011; Hisamori et al., 2008). However, this beneficial effect of ATRA is not seen in our NASH model. Hence, the molecular-cellular basis of the differential effect of ATRA in different liver injury models needs further exploration. Finally, our study shows that ATRA is decreased and Gas6 is increased in fibrotic livers, but the mechanisms of these changes remain unknown.

STAR★METHODS

Detailed methods are provided in the online version of this paper and include the following:

- KEY RESOURCES TABLE
- LEAD CONTACT AND MATERIALS AVAILABILITY
- EXPERIMENTAL MODEL AND SUBJECT DETAILS
  - Experimental Animals
  - Human Studies
- METHOD DETAILS
  - Assay of MerTK Cleavage
  - Flow Cytometry of Mouse Hepatic Cells
  - Preparation of Human Monocyte-Derived Macrophages and Mouse Bone Marrow-Derived Macrophages (BMDMs)
  - Isolation of Kupffer Cells
  - Isolation of Primary Hepatic Stellate Cells
  - Assay of Liver ATRA by LC/MS/MS
  - Quantification of Liver Fibrosis and Liver Macrophage MerTK Intensity
  - Quantification of Liver TUNEL$^+$ Cells and Efferocytosis
  - Immunoblotting
  - Quantitative RT-qPCR
  - siRNA-Mediated Gene Silencing
  - Analyses of Blood Glucose and Plasma Lipids and Liver Lipids
- QUANTIFICATION AND STATISTICAL ANALYSIS
- DATA AND CODE AVAILABILITY

SUPPLEMENTAL INFORMATION

Supplemental Information can be found online at https://doi.org/10.1016/j.cmet.2019.11.013.

ACKNOWLEDGMENTS

We thank Giorgio Rossi (Fondazione IRCCS Ca' Granda Ospedale Maggiore Policlinico Milano) for contributing to the evaluation of *MERTK* expression and activity in human liver cells. This work was supported, in part, by an American Heart Association Post-doctoral Fellowship grant (to B.C.); NIH grant 1K99DK115778 (to B.C.); an American Liver Foundation Liver Scholar Award (to X.W.); a Fellow Scholar Award from the American Society of Hematology (to Z.Z.); a Career Development Award from the American Heart Association (19CDA34660043) (to Z.Z.); NIH-NHLBI Post-doctoral Fellow institutional training grant T32HL007343 (to Z.Z.); NIH AI136715, DK108370, and DK078772 (to R.T.C.); the MGH Research Scholars Program (to R.T.C.); NIH grants DK068437 and DK101251 (to W.S.B.); NIH grant R01AI089824 (to C.V.R); NIH grant AI089824 (to C.V.R); C.V.R. is a Howard Hughes Medical Institute Faculty Scholar; MyFirst Grant Associazione Italiana per la Ricerca Sul Cancro (AIRC) n.16888 "EPIDEMIC-NAFLD" (to L.V.); Ricerca Finalizzata Ministero della Salute RF-2016-02364358 (to L.V.); Ricerca Corrente Fondazione IRCCS Ca' Granda Ospedale Maggiore Policlinico, (to L.V.); the European Union (EU) Programme Horizon 2020 (under grant agreement no. 777377) for the project LITMUS – "Liver Investigation: Testing Marker Utility in Steatohepatitis" (to L.V.); and NIH grants DK116620, HL132412, and HL087123 (to I.T.). The flow cytometric analyses used the Columbia Center for Translational Immunology/Diabetes and Endocrinology Research Center Flow Core facility, funded, in part, by NIH/National Institute of Diabetes and Digestive and Kidney Diseases Center grant 5P30DK063608.

AUTHOR CONTRIBUTIONS

B.C. and I.T. developed the study concept and experimental design; B.C. conducted all of the animal study procedures and the *in vitro* experiments; L.V. provided advice for the ideas and experiments related to *MERTK* polymorphisms and made available the human liver samples; P.D. and M.M. provided the liver samples and assayed the *MERTK* mRNA in human monocytes; X.W. provided advice on mouse NASH studies, made available the mouse liver samples, and helped with the Picosirius red quantification; R.F.S. provided advice related to the NASH fibrosis; I.O.S. and W.S.B. provided advice on the ATRA studies and conducted the liver ATRA assays using LC/MS-MS; K.E.C. and R.T.C. provided the human liver sections; C.K., V.D., and R.B.B. provided advice on the MerTK signaling and inhibition studies; R.B.B. made available the RU-301; Z.Z. provided advice related to how the *MERTK* SNPs may alter gene expression; B.C., R.F.S., W.S.B., L.V., and I.T. interpreted the data; B.C., L.V., and I.T. wrote the manuscript; and the other co-authors participated in the manuscript editing.

DECLARATION OF INTERESTS

The authors declare no competing interests.

Received: May 15, 2019
Revised: October 7, 2019
Accepted: November 13, 2019
Published: December 12, 2019

REFERENCES

Alsayed, Y., Uddin, S., Mahmud, N., Lekmine, F., Kalvakolanu, D.V., Minucci, S., Bokoch, G., and Platanias, L.C. (2001). Activation of Rac1 and the p38 mitogen-activated protein kinase pathway in response to all-trans-retinoic acid. J. Biol. Chem. *276*, 4012–4019.

Angulo, P., Kleiner, D.E., Dam-Larsen, S., Adams, L.A., Bjornsson, E.S., Charatcharoenwitthaya, P., Mills, P.R., Keach, J.C., Lafferty, H.D., Stahler, A., et al. (2015a). Liver fibrosis, but no other histologic features, is associated with long-term outcomes of patients with nonalcoholic fatty liver disease. Gastroenterology *149*, 389–397.e10.

Angulo, P., Machado, M.V., and Diehl, A.M. (2015b). Fibrosis in nonalcoholic fatty liver disease: mechanisms and clinical implications. Semin. Liver Dis. *35*, 132–145.

Bárcena, C., Stefanovic, M., Tutusaus, A., Joannas, L., Menéndez, A., García-Ruiz, C., Sancho-Bru, P., Marí, M., Caballeria, J., Rothlin, C.V., et al. (2015). Gas6/Axl pathway is activated in chronic liver disease and its targeting reduces fibrosis via hepatic stellate cell inactivation. J. Hepatol. *63*, 670–678.

Bartneck, M., Warzecha, K.T., and Tacke, F. (2014). Therapeutic targeting of liver inflammation and fibrosis by nanomedicine. Hepatobiliary Surg. Nutr. *3*, 364–376.

Baselli, G., and Valenti, L. (2019). Beyond fat accumulation, NAFLD genetics converges on lipid droplet biology. J. Lipid Res. *60*, 7–8.

Bellan, M., Cittone, M.G., Tonello, S., Rigamonti, C., Castello, L.M., Gavelli, F., Pirisi, M., and Sainaghi, P.P. (2019). Gas6/TAM system: a key modulator of the interplay between inflammation and fibrosis. Int. J. Mol. Sci. *20*, E5070.

Berry, D.C., and Noy, N. (2009). All-trans-retinoic acid represses obesity and insulin resistance by activating both peroxisome proliferation-activated receptor beta/delta and retinoic acid receptor. Mol. Cell. Biol. *29*, 3286–3296.

Birchenall-Roberts, M.C., Ruscetti, F.W., Kasper, J., Lee, H.D., Friedman, R., Geiser, A., Sporn, M.B., Roberts, A.B., and Kim, S.J. (1990). Transcriptional regulation of the transforming growth factor beta 1 promoter by v-src gene products is mediated through the AP-1 complex. Mol. Cell. Biol. *10*, 4978–4983.

Caballero, F., Fernández, A., De Lacy, A.M., Fernández-Checa, J.C., Caballería, J., and García-Ruiz, C. (2009). Enhanced free cholesterol, SREBP-2 and StAR expression in human NASH. J. Hepatol. *50*, 789–796.

Cai, B., Kasikara, C., Doran, A.C., Ramakrishnan, R., Birge, R.B., and Tabas, I. (2018). MerTK signaling in macrophages promotes the synthesis of inflammation resolution mediators by suppressing CaMKII activity. Sci. Signal. *11*, eaar3721.

Cai, B., Thorp, E.B., Doran, A.C., Sansbury, B.E., Daemen, M.J., Dorweiler, B., Spite, M., Fredman, G., and Tabas, I. (2017). MerTK receptor cleavage promotes plaque necrosis and defective resolution in atherosclerosis. J. Clin. Invest. *127*, 564–568.

Cai, B., Thorp, E.B., Doran, A.C., Subramanian, M., Sansbury, B.E., Lin, C.S., Spite, M., Fredman, G., and Tabas, I. (2016). MerTK cleavage limits proresolving mediator biosynthesis and exacerbates tissue inflammation. Proc. Natl. Acad. Sci. USA *113*, 6526–6531.

Camenisch, T.D., Koller, B.H., Earp, H.S., and Matsushima, G.K. (1999). A novel receptor tyrosine kinase, Mer, inhibits TNF-alpha production and lipopolysaccharide-induced endotoxic shock,. J. Immunol. *162*, 3498–3503.

Cavalli, M., Pan, G., Nord, H., Wallén Arzt, E., Wallerman, O., and Wadelius, C. (2017). Genetic prevention of hepatitis C virus-induced liver fibrosis by allele-specific downregulation of MERTK. Hepatol. Res. *47*, 826–830.

Chang, J., Thangamani, S., Kim, M.H., Ulrich, B., Morris, S.M., Jr., and Kim, C.H. (2013). Retinoic acid promotes the development of Arg1-expressing dendritic cells for the regulation of T-cell differentiation. Eur. J. Immunol. *43*, 967–978.

Chaves, G.V., Pereira, S.E., Saboya, C.J., Spitz, D., Rodrigues, C.S., and Ramalho, A. (2014). Association between liver vitamin A reserves and severity of nonalcoholic fatty liver disease in the class III obese following bariatric surgery. Obes. Surg. *24*, 219–224.

Ciuclan, L., Ehnert, S., Ilkavets, I., Weng, H.L., Gaitantzi, H., Tsukamoto, H., Ueberham, E., Meindl-Beinker, N.M., Singer, M.V., Breitkopf, K., et al. (2010). TGF-beta enhances alcohol dependent hepatocyte damage via down-regulation of alcohol dehydrogenase I. J. Hepatol. *52*, 407–416.

Clausen, B.E., Burkhardt, C., Reith, W., Renkawitz, R., and Förster, I. (1999). Conditional gene targeting in macrophages and granulocytes using LysMcre mice. Transgenic Res. *8*, 265–277.

Corey, K.E., and Kaplan, L.M. (2014). Obesity and liver disease: the epidemic of the twenty-first century. Clin. Liver Dis. *18*, 1–18.

Czochra, P., Klopcic, B., Meyer, E., Herkel, J., Garcia-Lazaro, J.F., Thieringer, F., Schirmacher, P., Biesterfeld, S., Galle, P.R., Lohse, A.W., et al. (2006). Liver fibrosis induced by hepatic overexpression of PDGF-B in transgenic mice. J. Hepatol. *45*, 419–428.

Dai, X., Yamasaki, K., Shirakata, Y., Sayama, K., and Hashimoto, K. (2004). All-trans-retinoic acid induces interleukin-8 via the nuclear factor-kappaB and p38 mitogen-activated protein kinase pathways in normal human keratinocytes. J. Invest. Dermatol. *123*, 1078–1085.

DeBerge, M., Yeap, X.Y., Dehn, S., Zhang, S., Grigoryeva, L., Misener, S., Procissi, D., Zhou, X., Lee, D.C., Muller, W.A., et al. (2017). MerTK cleavage on resident cardiac macrophages compromises repair after myocardial ischemia reperfusion injury. Circ. Res. *121*, 930–940.

Doycheva, I., Issa, D., Watt, K.D., Lopez, R., Rifai, G., and Alkhouri, N. (2018). Nonalcoholic steatohepatitis is the most rapidly increasing indication for liver transplantation in young adults in the United States. J. Clin. Gastroenterol. *52*, 339–346.

Dransfield, I., Zagórska, A., Lew, E.D., Michail, K., and Lemke, G. (2015). Mer receptor tyrosine kinase mediates both tethering and phagocytosis of apoptotic cells. Cell Death Dis. *6*, e1646.

Duffield, J.S., Forbes, S.J., Constandinou, C.M., Clay, S., Partolina, M., Vuthoori, S., Wu, S., Lang, R., and Iredale, J.P. (2005). Selective depletion of macrophages reveals distinct, opposing roles during liver injury and repair. J. Clin. Invest. *115*, 56–65.

Dulai, P.S., Singh, S., Patel, J., Soni, M., Prokop, L.J., Younossi, Z., Sebastiani, G., Ekstedt, M., Hagstrom, H., Nasr, P., et al. (2017). Increased risk of mortality by fibrosis stage in nonalcoholic fatty liver disease: systematic review and meta-analysis. Hepatology *65*, 1557–1565.

Fallowfield, J.A., Mizuno, M., Kendall, T.J., Constandinou, C.M., Benyon, R.C., Duffield, J.S., and Iredale, J.P. (2007). Scar-associated macrophages are a major source of hepatic matrix metalloproteinase-13 and facilitate the resolution of murine hepatic fibrosis. J. Immunol. *178*, 5288–5295.

Fourcot, A., Couchie, D., Chobert, M.N., Zafrani, E.S., Mavier, P., Laperche, Y., and Brouillet, A. (2011). Gas6 deficiency prevents liver inflammation, steatohepatitis, and fibrosis in mice. Am. J. Physiol. Gastrointest. Liver Physiol. *300*, G1043–G1053.

Fourgeaud, L., Través, P.G., Tufail, Y., Leal-Bailey, H., Lew, E.D., Burrola, P.G., Callaway, P., Zagórska, A., Rothlin, C.V., Nimmerjahn, A., et al. (2016). TAM receptors regulate multiple features of microglial physiology. Nature *532*, 240–244.

Gautier, E.L., Shay, T., Miller, J., Greter, M., Jakubzick, C., Ivanov, S., Helft, J., Chow, A., Elpek, K.G., Gordonov, S., et al. (2012). Gene-expression profiles and transcriptional regulatory pathways that underlie the identity and diversity of mouse tissue macrophages. Nat. Immunol. *13*, 1118–1128.

Gianni, M., Kopf, E., Bastien, J., Oulad-Abdelghani, M., Garattini, E., Chambon, P., and Rochette-Egly, C. (2002). Down-regulation of the phosphatidylinositol 3-kinase/Akt pathway is involved in retinoic acid-induced phosphorylation, degradation, and transcriptional activity of retinoic acid receptor gamma 2. J. Biol. Chem. *277*, 24859–24862.

Giannitrapani, L., Soresi, M., Bondì, M.L., Montalto, G., and Cervello, M. (2014). Nanotechnology applications for the therapy of liver fibrosis. World J. Gastroenterol. *20*, 7242–7251.

Gieseck, R.L., 3rd, Wilson, M.S., and Wynn, T.A. (2018). Type 2 immunity in tissue repair and fibrosis. Nat. Rev. Immunol. *18*, 62–76.

Hart, K.M., Fabre, T., Sciurba, J.C., Gieseck, R.L., 3rd, Borthwick, L.A., Vannella, K.M., Acciani, T.H., de Queiroz Prado, R., Thompson, R.W., White, S., et al. (2017). Type 2 immunity is protective in metabolic disease but exacerbates NAFLD collaboratively with TGF-beta. Sci. Transl. Med. *9*.

He, H., Mennone, A., Boyer, J.L., and Cai, S.Y. (2011). Combination of retinoic acid and ursodeoxycholic acid attenuates liver injury in bile duct-ligated rats and human hepatic cells. Hepatology *53*, 548–557.

Hisamori, S., Tabata, C., Kadokawa, Y., Okoshi, K., Tabata, R., Mori, A., Nagayama, S., Watanabe, G., Kubo, H., and Sakai, Y. (2008). All-trans-retinoic acid ameliorates carbon tetrachloride-induced liver fibrosis in mice through modulating cytokine production. Liver Int. *28*, 1217–1225.

Ioannou, G.N. (2016). The role of cholesterol in the pathogenesis of NASH. Trends Endocrinol. Metab. *27*, 84–95.

Jiménez-Sousa, M.Á., Gómez-Moreno, A.Z., Pineda-Tenor, D., Brochado-Kith, O., Sánchez-Ruano, J.J., Artaza-Varasa, T., Gómez-Sanz, A., Fernández-Rodríguez, A., and Resino, S. (2018). The myeloid-epithelial-reproductive tyrosine kinase (MERTK) rs4374383 polymorphism predicts

progression of liver fibrosis in hepatitis C virus-infected patients: a longitudinal study. J. Clin. Med. *7*, E473.

Jo, H., Mondal, S., Tan, D., Nagata, E., Takizawa, S., Sharma, A.K., Hou, Q., Shanmugasundaram, K., Prasad, A., Tung, J.K., et al. (2012). Small molecule-induced cytosolic activation of protein kinase Akt rescues ischemia-elicited neuronal death. Proc. Natl. Acad. Sci. USA *109*, 10581–10586.

Jolley, C.D., Dietschy, J.M., and Turley, S.D. (1999). Genetic differences in cholesterol absorption in 129/Sv and C57BL/6 mice: effect on cholesterol responsiveness. Am. J. Physiol. *276*, G1117–G1124.

Kane, M.A., Folias, A.E., Wang, C., and Napoli, J.L. (2008). Quantitative profiling of endogenous retinoic acid in vivo and in vitro by tandem mass spectrometry. Anal. Chem. *80*, 1702–1708.

Kasikara, C., Kumar, S., Kimani, S., Tsou, W.I., Geng, K., Davra, V., Sriram, G., Devoe, C., Nguyen, K.N., Antes, A., et al. (2017). Phosphatidylserine sensing by TAM receptors regulates AKT-dependent chemoresistance and PD-L1 expression. Mol. Cancer Res. *15*, 753–764.

Killock, D.J., and Ivetić, A. (2010). The cytoplasmic domains of TNFalpha-converting enzyme (TACE/ADAM17) and L-selectin are regulated differently by p38 MAPK and PKC to promote ectodomain shedding. Biochem. J. *428*, 293–304.

Kim, S.C., Kim, C.K., Axe, D., Cook, A., Lee, M., Li, T., Smallwood, N., Chiang, J.Y., Hardwick, J.P., Moore, D.D., et al. (2014). All-trans-retinoic acid ameliorates hepatic steatosis in mice by a novel transcriptional cascade. Hepatology *59*, 1750–1760.

Kimani, S.G., Kumar, S., Bansal, N., Singh, K., Kholodovych, V., Comollo, T., Peng, Y., Kotenko, S.V., Sarafianos, S.G., Bertino, J.R., et al. (2017). Small molecule inhibitors block Gas6-inducible TAM activation and tumorigenicity. Sci. Rep. *7*, 43908.

Lafdil, F., Chobert, M.N., Couchie, D., Brouillet, A., Zafrani, E.S., Mavier, P., and Laperche, Y. (2006). Induction of Gas6 protein in CCl4-induced rat liver injury and anti-apoptotic effect on hepatic stellate cells. Hepatology *44*, 228–239.

Lee, Y.J., Han, J.Y., Byun, J., Park, H.J., Park, E.M., Chong, Y.H., Cho, M.S., and Kang, J.L. (2012). Inhibiting Mer receptor tyrosine kinase suppresses STAT1, SOCS1/3, and NF-kappaB activation and enhances inflammatory responses in lipopolysaccharide-induced acute lung injury. J. Leukoc. Biol. *91*, 921–932.

Levi, L., Wang, Z., Doud, M.K., Hazen, S.L., and Noy, N. (2015). Saturated fatty acids regulate retinoic acid signalling and suppress tumorigenesis by targeting fatty acid-binding protein 5. Nat. Commun. *6*, 8794.

Liu, G., Ding, W., Liu, X., and Mulder, K.M. (2006). c-Fos is required for TGFbeta1 production and the associated paracrine migratory effects of human colon carcinoma cells. Mol. Carcinog. *45*, 582–593.

Liu, Y., Chen, H., Wang, J., Zhou, W., Sun, R., and Xia, M. (2015). Association of serum retinoic acid with hepatic steatosis and liver injury in nonalcoholic fatty liver disease. Am. J. Clin. Nutr. *102*, 130–137.

Liu, Z., Li, T., Jiang, K., Huang, Q., Chen, Y., and Qian, F. (2014). Induction of chemoresistance by all-trans retinoic acid via a noncanonical signaling in multiple myeloma cells. PLoS One *9*, e85571.

Machado, M.V., and Diehl, A.M. (2016). Pathogenesis of nonalcoholic steatohepatitis. Gastroenterology *150*, 1769–1777.

Mederacke, I., Dapito, D.H., Affò, S., Uchinami, H., and Schwabe, R.F. (2015). High-yield and high-purity isolation of hepatic stellate cells from normal and fibrotic mouse livers. Nat. Protoc. *10*, 305–315.

Milano, M., Dongiovanni, P., Artoni, A., Gatti, S., Rosso, L., Colombo, F., Bollati, V., Maggioni, M., Mannucci, P.M., Bertazzi, P.A., et al. (2016). Particulate matter phagocytosis induces tissue factor in differentiating macrophages. J. Appl. Toxicol. *36*, 151–160.

Monje, P., Hernández-Losa, J., Lyons, R.J., Castellone, M.D., and Gutkind, J.S. (2005). Regulation of the transcriptional activity of c-Fos by ERK. A novel role for the prolyl isomerase PIN1. J. Biol. Chem. *280*, 35081–35084.

Musso, G., Cassader, M., De Michieli, F., Paschetta, E., Pinach, S., Saba, F., Bongiovanni, D., Framarin, L., Berrutti, M., Leone, N., et al. (2017). MERTK rs4374383 variant predicts incident nonalcoholic fatty liver disease and diabetes: role of mononuclear cell activation and adipokine response to dietary fat. Hum. Mol. Genet. *26*, 1747–1758.

Nepal, S., Tiruppathi, C., Tsukasaki, Y., Farahany, J., Mittal, M., Rehman, J., Prockop, D.J., and Malik, A.B. (2019). STAT6 induces expression of Gas6 in macrophages to clear apoptotic neutrophils and resolve inflammation. Proc. Natl. Acad. Sci. USA *116*, 16513–16518.

Osawa, Y., Seki, E., Adachi, M., Suetsugu, A., Ito, H., Moriwaki, H., Seishima, M., and Nagaki, M. (2010). Role of acid sphingomyelinase of Kupffer cells in cholestatic liver injury in mice. Hepatology *51*, 237–245.

Patin, E., Kutalik, Z., Guergnon, J., Bibert, S., Nalpas, B., Jouanguy, E., Munteanu, M., Bousquet, L., Argiro, L., Halfon, P., et al. (2012). Genome-wide association study identifies variants associated with progression of liver fibrosis from HCV infection. Gastroenterology *143*, 1244–1252.e12.

Petta, S., Valenti, L., Marra, F., Grimaudo, S., Tripodo, C., Bugianesi, E., Cammà, C., Cappon, A., Di Marco, V., Di Maira, G., et al. (2016). MERTK rs4374383 polymorphism affects the severity of fibrosis in non-alcoholic fatty liver disease. J. Hepatol. *64*, 682–690.

Pingitore, P., Dongiovanni, P., Motta, B.M., Meroni, M., Lepore, S.M., Mancina, R.M., Pelusi, S., Russo, C., Caddeo, A., Rossi, G., et al. (2016). PNPLA3 overexpression results in reduction of proteins predisposing to fibrosis. Hum. Mol. Genet. *25*, 5212–5222.

Pradere, J.P., Kluwe, J., De Minicis, S., Jiao, J.J., Gwak, G.Y., Dapito, D.H., Jang, M.K., Guenther, N.D., Mederacke, I., Friedman, R., et al. (2013). Hepatic macrophages but not dendritic cells contribute to liver fibrosis by promoting the survival of activated hepatic stellate cells in mice. Hepatology *58*, 1461–1473.

Puche, J.E., Saiman, Y., and Friedman, S.L. (2013). Hepatic stellate cells and liver fibrosis. Compr. Physiol. *3*, 1473–1492.

Puri, P., Baillie, R.A., Wiest, M.M., Mirshahi, F., Choudhury, J., Cheung, O., Sargeant, C., Contos, M.J., and Sanyal, A.J. (2007). A lipidomic analysis of nonalcoholic fatty liver disease. Hepatology *46*, 1081–1090.

Ramachandran, P., Dobie, R., Wilson-Kanamori, J.R., Dora, E.F., Henderson, B.E.P., Luu, N.T., Portman, J.R., Matchett, K.P., Brice, M., Marwick, J.A., et al. (2019). Resolving the fibrotic niche of human liver cirrhosis at single-cell level. Nature *575*, 512–518.

Ren, X., Li, Y., Ma, X., Zheng, L., Xu, Y., and Wang, J. (2007). Activation of p38/MEF2C pathway by all-trans retinoic acid in cardiac myoblasts. Life Sci. *81*, 89–96.

Rinella, M.E. (2015). Nonalcoholic fatty liver disease: a systematic review. JAMA *313*, 2263–2273.

Rinella, M.E., and Sanyal, A.J. (2016). Management of NAFLD: a stage-based approach. Nat. Rev. Gastroenterol. Hepatol. *13*, 196–205.

Romeo, S., and Valenti, L. (2016). Regulation of retinol-binding protein 4 and retinol metabolism in fatty liver disease. Hepatology *64*, 1414–1416.

Sather, S., Kenyon, K.D., Lefkowitz, J.B., Liang, X., Varnum, B.C., Henson, P.M., and Graham, D.K. (2007). A soluble form of the Mer receptor tyrosine kinase inhibits macrophage clearance of apoptotic cells and platelet aggregation. Blood *109*, 1026–1033.

Schwabe, R.F., and Luedde, T. (2018). Apoptosis and necroptosis in the liver: a matter of life and death. Nature reviews. Nat. Rev. Gastroenterol. Hepatol. *15*, 738–752.

Scott, R.S., McMahon, E.J., Pop, S.M., Reap, E.A., Caricchio, R., Cohen, P.L., Earp, H.S., and Matsushima, G.K. (2001). Phagocytosis and clearance of apoptotic cells is mediated by MER. Nature *411*, 207–211.

Spite, M. (2019). Resolving inflammation in nonalcoholic steatohepatitis. J. Clin. Invest. *130*, 1524–1526.

Subramanian, M., Thorp, E., Hansson, G.K., and Tabas, I. (2013). Treg-mediated suppression of atherosclerosis requires MYD88 signaling in DCs. J. Clin. Invest. *123*, 179–188.

Thorp, E., Cui, D., Schrijvers, D.M., Kuriakose, G., and Tabas, I. (2008). Mertk receptor mutation reduces efferocytosis efficiency and promotes apoptotic cell accumulation and plaque necrosis in atherosclerotic lesions of apoe-/- mice. Arterioscler. Thromb. Vasc. Biol. *28*, 1421–1428.

Thorp, E., Vaisar, T., Subramanian, M., Mautner, L., Blobel, C., and Tabas, I. (2011). Shedding of the Mer tyrosine kinase receptor is mediated by ADAM17 protein through a pathway involving reactive oxygen species, protein kinase Cδ, and p38 mitogen-activated protein kinase (MAPK). J. Biol. Chem. *286*, 33335–33344.

Tibrewal, N., Wu, Y., D'Mello, V., Akakura, R., George, T.C., Varnum, B., and Birge, R.B. (2008). Autophosphorylation docking site Tyr-867 in Mer receptor tyrosine kinase allows for dissociation of multiple signaling pathways for phagocytosis of apoptotic cells and down-modulation of lipopolysaccharide-inducible NF-kappaB transcriptional activation. J. Biol. Chem. *283*, 3618–3627.

Tomita, K., Teratani, T., Suzuki, T., Oshikawa, T., Yokoyama, H., Shimamura, K., Nishiyama, K., Mataki, N., Irie, R., Minamino, T., et al. (2012). p53/p66Shc-mediated signaling contributes to the progression of non-alcoholic steatohepatitis in humans and mice. J. Hepatol. *57*, 837–843.

Triantafyllou, E., Pop, O.T., Possamai, L.A., Wilhelm, A., Liaskou, E., Singanayagam, A., Bernsmeier, C., Khamri, W., Petts, G., Dargue, R., et al. (2018). MerTK expressing hepatic macrophages promote the resolution of inflammation in acute liver failure. Gut *67*, 333–347.

Tsou, W.I., Nguyen, K.Q., Calarese, D.A., Garforth, S.J., Antes, A.L., Smirnov, S.V., Almo, S.C., Birge, R.B., and Kotenko, S.V. (2014). Receptor tyrosine kinases, TYRO3, AXL, and MER, demonstrate distinct patterns and complex regulation of ligand-induced activation. J. Biol. Chem. *289*, 25750–25763.

Tsuchida, T., and Friedman, S.L. (2017). Mechanisms of hepatic stellate cell activation. Nat. Rev. Gastroenterol. Hepatol. *14*, 397–411.

Tutusaus, A., de Gregorio, E., Cucarull, B., Cristóbal, H., Aresté, C., Graupera, I., Coll, M., Colell, A., Gausdal, G., Lorens, J.B., et al. (2019). A functional role of Gas6/TAM in non-alcoholic steatohepatitis progression implicates Axl as therapeutic target. Cell. Mol. Gastroenterol. Hepatol. Published online November 2, 2019. https://doi.org/10.1016/j.jcmgh.2019.10.010.

Ukleja, A., Scolapio, J.S., McConnell, J.P., Spivey, J.R., Dickson, R.C., Nguyen, J.H., and O'Brien, P.C. (2002). Nutritional assessment of serum and hepatic vitamin A levels in patients with cirrhosis. JPEN J. Parenter. Enteral. Nutr. *26*, 184–188.

Vander Ark, A., Cao, J., and Li, X. (2018). TGF-β receptors: in and beyond TGF-β signaling. Cell. Signal. *52*, 112–120.

Vilar-Gomez, E., Calzadilla-Bertot, L., Wai-Sun Wong, V., Castellanos, M., Aller-de la Fuente, R., Metwally, M., Eslam, M., Gonzalez-Fabian, L., Alvarez-Quiñones Sanz, M., Conde-Martin, A.F., et al. (2018). Fibrosis severity as a determinant of cause-specific mortality in patients with advanced nonalcoholic fatty liver disease: a multi-national cohort study. Gastroenterology *155*, 443–457.e17.

Vogel, S., Piantedosi, R., Frank, J., Lalazar, A., Rockey, D.C., Friedman, S.L., and Blaner, W.S. (2000). An immortalized rat liver stellate cell line (HSC-T6): a new cell model for the study of retinoid metabolism in vitro. J. Lipid Res. *41*, 882–893.

Wang, X., Zheng, Z., Caviglia, J.M., Corey, K.E., Herfel, T.M., Cai, B., Masia, R., Chung, R.T., Lefkowitch, J.H., Schwabe, R.F., et al. (2016). Hepatocyte TAZ/WWTR1 promotes inflammation and fibrosis in nonalcoholic steatohepatitis. Cell Metab. *24*, 848–862.

Weiskirchen, R., and Tacke, F. (2016). Liver fibrosis: from pathogenesis to novel therapies. Dig. Dis. *34*, 410–422.

Xiong, X., Kuang, H., Ansari, S., Liu, T., Gong, J., Wang, S., Zhao, X.Y., Ji, Y., Li, C., Guo, L., et al. (2019). Landscape of intercellular crosstalk in healthy and NASH liver revealed by single-cell secretome gene analysis. Mol. Cell *75*, 644–660.e5.

Xu, P., and Derynck, R. (2010). Direct activation of TACE-mediated ectodomain shedding by p38 MAP kinase regulates EGF receptor-dependent cell proliferation. Mol. Cell *37*, 551–566.

Xu, P., Liu, J., Sakaki-Yumoto, M., and Derynck, R. (2012). TACE activation by MAPK-mediated regulation of cell surface dimerization and TIMP3 association. Sci. Signal. *5*, ra34.

Yang, L., Roh, Y.S., Song, J., Zhang, B., Liu, C., Loomba, R., and Seki, E. (2014). Transforming growth factor beta signaling in hepatocytes participates in steatohepatitis through regulation of cell death and lipid metabolism in mice. Hepatology *59*, 483–495.

Zheng, Q.F., Bai, L., Duan, Z.P., Han, Y.P., Zheng, S.J., Chen, Y., and Li, J.S. (2017). M2-like Kupffer cells in fibrotic liver may protect against acute insult. World J. Gastroenterol. *23*, 3655–3663.

STAR★METHODS

KEY RESOURCES TABLE

REAGENT or RESOURCE	SOURCE	IDENTIFIER
Antibodies		
Goat anti-mouse MerTK	R&D Systems	Cat# AF591; RRID:AB_2098565 (1:1000 dilution)
Goat anti-mouse Axl	R&D Systems	Cat# AF854; RRID:AB_355663 (1:1000 dilution)
Goat anti-mouse CLEC4F	R&D Systems	Cat# AF2784; RRID:AB_2081339 (1:200 dilution)
Mouse anti-human TGF-beta1	R&D Systems	Cat# MAB240; RRID:AB_358119 (1:50 dilution)
Mouse anti-human CD68 antibody	Agilent	Cat# M0814; RRID:AB_2314148 (1:300 dilution)
Rabbit anti-phospho Smad2/3	Cell Signaling Technology	Cat# 8828; RRID:AB_2631089 (1:1000 dilution)
Rabbit anti-Smad2/3	Cell Signaling Technology	Cat# 8685; RRID:AB_10889933 (1:1000 dilution)
Rabbit anti-phospho P38	Cell Signaling Technology	Cat# 4631; RRID:AB_331765 (1:1000 dilution)
Rabbit anti-P38	Cell Signaling Technology	Cat# 8690; RRID:AB_10999090 (1:1000 dilution)
Rabbit anti-phospho AKT	Cell Signaling Technology	Cat# 4060; RRID:AB_2315049 (1:1000 dilution)
Rabbit anti-AKT	Cell Signaling Technology	Cat# 4685; RRID:AB_2225340 (1:1000 dilution)
Rabbit anti-beta actin (HRP)	Cell Signaling Technology	Cat# 5125; RRID:AB_1903890 (1:5000 dilution)
Rabbit anti-Smad2/3 (PE)	Cell Signaling Technology	Cat# 72255; RRID:AB_2799818 (1:100 dilution)
Rabbit anti-ERK1/2 (PE)	Cell Signaling Technology	Cat# 8867; RRID:AB_2797675 (1:100 dilution)
Rat anti-mouse MerTK (PE)	eBiosciences	Cat# 12-5751-80; RRID:AB_2572622 (1:100 dilution)
Rabbit anti-ADAM17	Sigma-Aldrich	Cat# T5442; RRID:AB_1840689 (1:1000 dilution)
Goat anti-mouse (CF555)	Sigma-Aldrich	Cat# SAB4600066; RRID:AB_2336060 (1:500 dilution)
Goat anti-rabbit (CF647)	Sigma-Aldrich	Cat# SAB4600184; RRID:AB_2665437 (1:500 dilution)
Mouse anti-alpha-smooth muscle actin (Cy3)	Sigma-Aldrich	Cat# C6198; RRID:AB_476856 (1:300 dilution)
Donkey anti-rabbit (HRP)	Jackson ImmunoResearch Labs	Cat# 711-035-152; RRID:AB_10015282 (1:5000 dilution)
Mouse anti-goat (HRP)	Santa Cruz Biotechnology	Cat# sc-2354; RRID:AB_628490 (1:5000 dilution)
Rat anti-mouse CD16/CD32	BD Biosciences	Cat# 553142; RRID:AB_394657 (1:100 dilution)
Mouse anti-phospho Smad2/3 (AF647)	BD Biosciences	Cat# 562696; RRID:AB_2716578 (1:500 dilution)
Rabbit anti-human MerTK antibody	Abcam	Cat# ab52968; RRID:AB_2143584 (1:1000 dilution)

(*Continued on next page*)

Continued

REAGENT or RESOURCE	SOURCE	IDENTIFIER
Goat anti-RAR alpha	Abcam	Cat# ab28767; RRID:AB_777684 (1:500 dilution)
Rabbit anti-RAR beta	Abcam	Cat# ab53161; RRID:AB_882283 (1:500 dilution)
Rat anti-mouse CD45 (APC)	Biolegend	Cat# 103112; RRID:AB_312977 (1:100 dilution)
Rat anti-mouse F4/80 (PE/Cy7)	Biolegend	Cat# 123113; RRID:AB_893490 (1:100 dilution)
Rat anti-mouse CD11b (AF488)	Biolegend	Cat# 101217; RRID:AB_389305 (1:100 dilution)
Mouse anti-mouse LAP (APC)	Biolegend	Cat# 141405; RRID:AB_10896418 (1:100 dilution)
Mouse anti-phospho ERK1/2 (PE)	Biolegend	Cat# 369506; RRID:AB_2629705 (1:100 dilution)
Rabbit anti-F4/80	GeneTex	Cat# GTX101895; RRID:AB_1950198 (1:1000 dilution)
Chemicals, Peptides, and Recombinant Proteins		
Dulbecco's Modified Eagle Media (DMEM)	Corning	Cat# 10-013-CV
Roswell Park Memorial Institute (RPMI) 1640 Media	Corning	Cat# 10-040-CV
1X PBS	Corning	Cat# 21-040-CV
CellStripper	Corning	Cat# 25-056-CI
Penicillin/Streptomycin	Corning	Cat# 30-002-CI
10X Tris-buffered saline	Corning	Cat# 46-012-CM
Heat-Inactivated Fetal Bovine Serum	GIBCO	Cat# 10438-026
Opti-MEM	GIBCO	Cat# 31985-070
Human Granulocyte Colony Stimulating Factor (GM-CSF)	PeproTech	Cat# 300-03
HISTOPAQUE	Sigma-Aldrich	Cat# 10771
Citrate-dextrose solution	Sigma-Aldrich	Cat# C3821
Collagenase I	Sigma-Aldrich	Cat# 1148089
DMSO	Sigma-Aldrich	Cat# D2650
All-trans retinoic acid (ATRA)	Sigma-Aldrich	Cat# R2625
Protease from Streptomyces griseus	Sigma-Aldrich	Cat# P5147
Gey's Balanced Salt Solution	Sigma-Aldrich	Cat# G9779
Collagenase D	Roche	Cat# 11088866001
Recombinant mouse Gas6 protein	R&D Systems	Cat# 986-GS
AGN193109	R&D Systems	Cat# 5758
SC79	R&D Systems	Cat# 4635
TAPI-0	R&D Systems	Cat# 5523
Recombinant human Mer-FC chimeric protein (sol-Mer)	R&D Systems	Cat# 891-MR-100
Recombinant human protein S	Haematologic Technologies	Cat# HCPS-0090
SB203580	Selleckchem	Cat# S1076
BMS-777607	Selleckchem	Cat# S1561
Novex 4–20% Tris-Glycine Mini Gels, 15-well	Invitrogen	Cat# XP04205BOX
DAPI Nucleic Acid Stain	Invitrogen	Cat# P36934
4X Laemmli Buffer	Bio-Rad	Cat# 161-0747
2X Laemmli Buffer	Bio-Rad	Cat# 161-0737
β-mercaptoethanol	Bio-Rad	Cat# 1610710

(*Continued on next page*)

Continued

REAGENT or RESOURCE	SOURCE	IDENTIFIER
0.45-μm nitrocellulose membranes	Bio-Rad	Cat# 1620115
Hoechst 33342	Thermo Scientific	Cat# 62249
Lipofectamine RNAiMax	Life Technologies	Cat# 13778-150
Lymphoprep™	Stemcell Technologies	Cat# 07851
Power SYBR Green PCR Master Mix	Applied Biosystems	Cat# 4367659
40 μm Nylon Cell Strainers	Fisher Scientific	Cat# 22363547
100 μm Nylon Cell Strainers	Fisher Scientific	Cat# 22363549
70 μm Nylon Cell Strainers	Falcon	Cat# 352350
FACS-staining buffer	BD Biosciences	Cat# 554656
Perm buffer II	BD Biosciences	Cat# 558052
Anti-mouse F4/80 microbeads	MACS	Cat#130-110-443
Nycodenz	Accurate Chemical	Cat# AN1002423
ATRA-d5	Toronto Research Chemicals	Cat# R250202
RIPA buffer	Thermo Fisher Scientific	Cat# 89900
Human Gas6-conditioned media	Tsou et al., 2014	N/A
Critical Commercial Assays		
Picrosirius (Sirius) Red Stain Kit	Polysciences	Cat# 24901
ALT Test Kit	TECO Diagnostics	Cat# A526-120
RNeasy Mini Kit	Qiagen	Cat# 74106
TUNEL Kit	Roche	Cat# 12156792910
Mouse Mer DuoSet ELISA Kit	R&D Systems	Cat# DY591
SensoLyte® 520 TACE (α-secretase) Activity Assay Kit	AnaSpec	Cat# AS-72085
Hydroxyproline Kit	Sigma-Aldrich	Cat# MAK008
Total Cholesterol Kit	Wako Diagnostics	Cat# 999-02601
Triglycerides Kit Color A	Wako Diagnostics	Cat# 994-02891
Triglycerides Kit Color B	Wako Diagnostics	Cat# 990-02991
BCA assay	Thermo Fisher Scientific	Cat# 23227
Supersignal West Pico Chemiluminescence Kit	Thermo Fisher Scientific	Cat# 34080
Experimental Models: Cell Lines		
Mouse: L-929 fibroblast cells	ATCC	ATCC CCL-1
Mouse: Bone marrow-derived macrophage cells	This paper	N/A
Mouse: Kupffer cells	This paper	N/A
Human: Peripheral blood monocyte-derived macrophage cells	This paper	N/A
Rat: HSC-T6	Vogel et al., 2000	N/A
Experimental Models: Organisms/Strains		
Mouse: C57BL/6J	The Jackson Laboratory	JAX: 000664
Mouse: $Mertk^{-/-}$: C57Bl/6J	Thorp et al., 2008	N/A
Mouse: $Mertk^{CR}$: C57Bl/6J	Cai et al., 2016	N/A
Mouse: $Mertk^{fl/fl}$: C57Bl/6J	Fourgeaud et al., 2016	N/A
Mouse: Lyz2cre: C57Bl/6J	Clausen et al., 1999	N/A
Oligonucleotides		
ON-TARGET plus non-targeting pool	GE Healthcare Dharmacon	D-001810-10-05
Human: MERTK SMARTpool	GE Healthcare Dharmacon	L-003155-00-0010
Human: MAPK1/3	Cell Signaling Technology	Cat# 6560
Mouse: Mertk SMARTpool	GE Healthcare Dharmacon	L-040357-00-0010

(*Continued on next page*)

Continued

REAGENT or RESOURCE	SOURCE	IDENTIFIER
Mouse: Rara SMARTpool	GE Healthcare Dharmacon	L-047625-02-0005
Mouse: Rarb SMARTpool	GE Healthcare Dharmacon	L-040538-00-0005
Software and Algorithms		
Leica Application Suite	Leica	Advanced Fluorescence
ImageJ	NIH	www.imagej.nih.gov/ij
PRISM	GraphPad Software	Version 6
FlowJo	FlowJo	Version 10
Other		
Mouse Diet: NASH Diet	Envigo	Cat# TD.190142
Genotyping Service	Genetyper	www.genetyper.com

LEAD CONTACT AND MATERIALS AVAILABILITY

Further information and requests for resources and reagents should be directed to and will be fulfilled by the Lead Contact, Dr. Ira Tabas (iat1@columbia.edu). This study did not generate new unique reagents.

EXPERIMENTAL MODEL AND SUBJECT DETAILS

Experimental Animals

Mertk$^{-/-}$, *Mertk*^{CR}, *Mertk*$^{fl/fl}$, and *Lyz2cre* male mice on the C57BL6/J background were generated as previously described (Cai et al., 2016; Clausen et al., 1999; Fourgeaud et al., 2016; Thorp et al., 2008). Male wild-type C57BL/6J mice (10-12 weeks/old) were obtained from Jackson Laboratory (Bar Harbor, ME) and were allowed to adapt to housing in the animal facility for 1 week before the commencement of experiments. The mice were fed a NAFLD-inducing diet (Envigo, TD.190142: 1.25% cholesterol and 8.7% palmitic acid with drinking water containing 23.1 g/L fructose and 18.9 g/L glucose) or control diet (LabDiet Rodent Diet 20, #5053: 0.01% cholesterol and 0% palmitic acid) for the times indicated in the figure legends, as previously described and validated in detail (Wang et al., 2016). Hepatosteatosis is observed after 8 weeks of diet feeding, and inflammation, cell death, and early fibrosis are evident by 16 weeks. The high percentage of cholesterol in the diet is necessary to achieve an increase in liver cholesterol similar to that observed in human NASH liver (Caballero et al., 2009; Ioannou, 2016; Puri et al., 2007), taking into account the fact that C57BL/6J mice absorb cholesterol relatively poorly (Jolley et al., 1999). For RU-301 experiment, RU-301 was synthesized as described (Kimani et al., 2017), dissolved in DMSO (Sigma Aldrich), and injected i.p. at a dose of 300 mg/kg body weight three times a week for 4 weeks. For the ATRA administration experiment, ATRA (Sigma Aldrich) was dissolved in coconut oil and was injected i.p. at a dose of 15 μg/gram body weight of mice, three times a week for 8 weeks. Fasting blood glucose was measured using a glucose meter (One Touch Ultra, Life- scan) after withdrawal of food for 5 h, with free access to water. Some aliquots of liver were fixed in 10% formalin, embedded in paraffin, and sectioned for histology analysis, followed by lipid droplet area analysis and Sirius red staining, which were quantified using ImageJ. Other aliquots were either snap-frozen for gene expression analysis or mechanically dissociated for flow cytometry. Animals were housed in standard cages at 22°C in a 12-12 h light-dark cycle in a barrier facility. All animal experiments were performed by following institutional guidelines and regulations and approved by the Institutional Animal Care and Use Committee at Columbia University.

Human Studies

For the analysis of *MERTK* mRNA expression levels in peripheral blood monocytes carrying *MERTK* rs4374383 GG, GA and AA genotypes, monocytes were isolated from healthy subjects with normal coagulation and iron metabolism parameters and without cardiovascular disease. Mononuclear cells (monocytes and lymphocytes) were isolated from 200 ml of blood that was anti-coagulated using 3.2% citrate using Lymphoprep™ (Stemcell Technologies), according to the manufacturer's instructions. In this procedure, erythrocytes and the PMNs sediment through the medium (density 1.077 g/ml), while mononuclear cells are retained at the sample/medium interface, as previously described (Milano et al., 2016). Isolated mononuclear cells were cultured in RPMI 1640 medium supplemented with 10% FBS, 1% β-mercaptoethanol, and 1% glutamine. After 24 h, non-adherent lymphocytes were removed, leaving behind adherent monocytes. RNA in adherent monocytes was extracted for *MERTK* mRNA qPCR assay, and DNA was assessed by MERTK genotype at rs4374383. For the analysis of liver MerTK staining in NASH patients carrying *MERTK* rs4374383 GG, GA and AA genotypes, liver biopsy specimens were fixed in 10% formalin, embedded in paraffin, and sectioned. For both studies, written informed consent was obtained from each subject, and the studies were approved by the Institutional Review Board of the Fondazione IRCCS Ca' Granda.

To assess MerTK staining in macrophages in control, steatotic, and NASH fibrotic liver sections, liver biopsy specimens from individuals undergoing weight loss surgery were selected from the MGH NAFLD Biorepository. Patients gave informed consent at

the time of recruitment, and their records were anonymized and de-identified, and studies were approved by the Partners Human Research Committee. The sections, which were characterized by a liver pathologist as being most representative of normal, steatosis, or NASH fibrosis, were stained with mouse anti-human CD68 and rabbit anti-human MerTK, followed by addition of secondary antibodies. The slides were counterstained with DAPI Nucleic Acid Stain (Invitrogen). Liver MerTK intensity in $CD68^+$ cells was analyzed under a Leica fluorescent microscope (Leica Microsystems, Germany). All human studies were approved by the Columbia University Institutional Review Board and were conducted in accordance with National Institutes of Health and institutional guidelines for human subject research.

METHOD DETAILS

Assay of MerTK Cleavage

Aliquots of mouse liver (~150 mg) were placed in 40-μm cell strainers and gently homogenized with 1 ml 1X PBS. Homogenates were centrifuged at 1000 x g for 10 min at 4°C. Supernatant fractions were lysed with 4X Laemmli buffer (Bio-Rad) containing 5% β-mercaptoethanol (Bio-Rad) and immunoblotted for sol-Mer, and cell pellets were lysed and immunoblotted for MerTK and β-actin. Sol-Mer was detected in human liver specimens obtained from morbidly obese individuals who underwent percutaneous liver biopsy performed during bariatric surgery. These subjects had no history of alcohol abuse (<30 g/day for males and <20 g/day for females) or other liver diseases. NASH was diagnosed when steatosis, lobular inflammation, and ballooning were concomitantly present. Informed written consent was obtained from each patient. The study protocol was approved by the Ethical Committee of the Fondazione IRCCS Ca' Granda, Milan and conforms to the ethical guidelines of the 1975 Declaration of Helsinki. Hepatic samples with a length of 1.5 cm were directly lysed in SDS buffer, containing 1 mmol/L Na-orthovanadate, 200 mmol/L phenylmethyl sulfonyl fluoride, and 0.02 μg/μL aprotinin. Equal amounts of protein (~10 μg) were separated by SDS-PAGE and immunoblotted for sol-Mer, MerTK, and β-actin. For assay of MerTK cleavage in macrophages, mouse BMDMs were cultured in DMEM media containing 3% FBS for 4 h. The cells were then washed with PBS and incubated for 3 h with DMSO (vehicle) or 10 μM ATRA in medium containing 3% FBS. Culture media were collected and assayed for sol-Mer measurement by ELISA.

Flow Cytometry of Mouse Hepatic Cells

Liver tissue (~150 mg) was excised and mechanically dissociated in 1X PBS and passed through a 100 μm cell strainer. The cell suspension was centrifuged at 60 x g for 1 min to pellet hepatocytes, which were used for flow cytometric analysis. For cell-surface protein staining, cells were blocked with anti-mouse CD16/CD32 antibody (BD Biosciences) and were then stained with the indicated antibodies for 1 h in FACS-staining buffer (BD Biosciences). For staining of intracellular proteins, cells were fixed with 2% paraformaldehyde (PFA) for 10 min and permeabilized with buffer (BD Biosciences) for 1 h, followed by incubation with the indicated antibodies. Flow cytometric assessment was conducted using a FACSCanto II (BD Biosciences), and data were analyzed using FlowJo software (Tree Star).

Preparation of Human Monocyte-Derived Macrophages and Mouse Bone Marrow-Derived Macrophages (BMDMs)

To generate human macrophages, peripheral human blood leukocytes were isolated from the buffy coats of de-identified healthy volunteers (New York Blood Center). Buffy coats were gently layered onto Histopaque solution (Sigma Aldrich) as 1:1 ratio (vol/vol) and centrifuged at 1,500 x g for 25 min. Leukocytes were removed from the middle layer, washed with RPMI medium, and then centrifuged at 1,500 x g for 5 minutes. This wash step was repeated once, and then the cell pellet was suspended in RPMI medium and plated into 12-well plates. After 3 to 4 hours, when monocytes were adherent, the medium was exchanged for RPMI containing 10% (vol/vol) FBS, 1% pen-strep, and 10 ng/ml recombinant human GM-CSF (PeproTech), and the cells were incubated for 7 to 10 days to allow macrophage differentiation. To generate mouse BMDMs, bone marrow cells from 8-12 week old mice were cultured for 7-10 days in DMEM supplemented with 10% (vol/vol) FBS, 1% pen-strep, and 20% (vol/vol) L-929 fibroblast-conditioned media.

Isolation of Kupffer Cells

As described previously (Wang et al., 2016), mice were euthanized with isoflurane, and a cannula was inserted into the inferior vena cava. The portal vein was cut, and the liver was perfused sequentially through the vena cava cannula with solutions containing protease from *Streptomyces griseus* (14 mg/mouse, Sigma Aldrich) and collagenase D (3.7 U/mouse, Roche). Digested liver was generally disrupted using a tissue homogenizer, and the resulting cell suspension was centrifuged at 60 x g for 1 min to pellet hepatocytes. Kupffer cells in the supernatant fraction were then isolated by using anti-F4/80 microbeads (MACS) and cultured in DMEM containing 10% (vol/vol) FBS and 1% pen-strep.

Isolation of Primary Hepatic Stellate Cells

HSCs were isolated from 5-6 mo/o BALB/C mice as described previously (Mederacke et al., 2015; Wang et al., 2016). After cannulation of the inferior vena cava, the portal vein was cut, followed by retrograde step-wise perfusion with solutions containing protease (14 mg/mouse, Sigma Aldrich) and collagenase D (3.7 U/mouse, Roche). Livers were then minced with forceps. The minced livers were further digested in the solution containing 1% DNase, protease (25 mg/mouse) and collagenase D (4.4 U/mouse) for 25 min. Digested livers were filtered through a 70-μm cell strainer to get rid of non-digested tissue. The cell suspensions were centrifuged

at 580 x g for 10 min at 4°C. Cell pellets were washed with Gey's Balanced Salt Solution (Sigma Aldrich) twice. Cells were then subjected to gradient centrifugation on 9.7% Nycodenz (Accurate Chemical) to isolate HSCs, which were then plated in tissue culture dishes in DMEM containing 10% (vol/vol) FBS and 1% pen-strep.

Assay of Liver ATRA by LC/MS/MS

Liver tissue (> 120 mg) was collected in 4 volumes of 50% ethanol, disrupted by homogenization, and extracted using the two-step acid-base extraction described by Kane et al (Kane et al., 2008). Initially,12.5 μL of 2 M KOH in ethanol was added to a 20% (wt/vol) tissue homogenate, along with 10 ng of penta-deuterated all-*trans*-retinoic acid (ATRA-d5) (Toronto Research Chemicals, Ontario, Canada) dissolved in absolute ethanol to serve as an internal standard. The aqueous phase containing non-polar lipids was then extracted with hexane. The remaining aqueous phase was acidified with 50 μL of 8 M HCl and polar lipids including ATRA were extracted with hexane. The hexane extract containing ATRA was dried under N_2 and suspended in acetonitrile for LC/MS/MS analysis using a Waters Xevo TQ MS ACQUITY UPLC system (Waters, Milford, MA). ATRA was detected and quantified using the multiple reaction monitoring mode employing the following transitions: ATRA, m/z 301.16 → 123.00; penta-deuterated ATRA, m/z 306.15 → 127.03; and 9-cis-RA, m/z 301.16 → 123.00.

Quantification of Liver Fibrosis and Liver Macrophage MerTK Intensity

Liver fibrosis was detected with Sirius red staining according to the manufacturer's instructions and quantified as % Sirius red$^+$ area of total area by ImageJ. Liver macrophage MerTK intensity was assayed by co-staining sections with anti-CD68 (1:300) and anti-MerTK (1:200) antibodies. MerTK intensity in CD68$^+$ cells was assayed using immunofluorescence microscopy and quantified by ImageJ. The same threshold settings were used for all analyses.

Quantification of Liver TUNEL$^+$ Cells and Efferocytosis

Liver sections were stained with TUNEL (Roche) followed by anti-F4/80 to label macrophages. In situ efferocytosis in liver was quantified as previously described for atherosclerotic lesions (Subramanian et al., 2013; Thorp et al., 2008). TUNEL$^+$ cells were determined to be either macrophage-associated (co-localizing or juxtaposed with macrophages) or free (not associated with macrophages). Data are plotted as a ratio of associated:free cells to represent efferocytosis efficiency. Images were captured using a Zeiss fluorescence microscope and analyzed using FIJI/ImageJ by an observer blinded to the group assignment of each sample.

Immunoblotting

Liver protein lysates were extracted using RIPA buffer (Thermo Fisher Scientific), and the protein concentration was measured using the BCA assay (Thermo Fisher Scientific). Proteins were separated by electrophoresis on 4-20% Tris gels (Invitrogen) and transferred to 0.45-μm nitrocellulose membranes (Bio-Rad). The membranes were blocked for 1 h at room temperature in Tris-buffered saline/0.1% Tween 20 (TBST) containing 5% (wt/vol) nonfat milk and then incubated with the primary antibody in TBST containing 5% (wt/vol) nonfat milk or 5% (wt/vol) BSA at 4°C overnight. The membranes were then incubated with the appropriate secondary antibody coupled to horseradish peroxidase, and proteins were detected by the ECL Supersignal West Pico chemiluminescence kit (Thermo Fisher Scientific). Cultured cells were lysed in 2X Laemmli buffer (Bio-Rad) containing 5% β-mercaptoethanol, heated at 100°C for 5 min, and then electrophoresed and immunoblotted as above.

Quantitative RT-qPCR

Total RNA was extracted from liver tissue or cultured macrophages using the RNeasy kit (Qiagen). The quality and concentration of the RNA was assessed by absorbance at 260 and 280 nm using a NanoDrop spectrophotometer (Thermo Fisher Scientific). cDNA was synthesized from 0.5-1 μg RNA using oligo (dT) and Superscript II (Applied Biosystems). Quantitative RT-PCR was performed with a 7500 Real-time PCR system (Applied Biosystems) using SYBR green chemistry (Applied Biosystems). The primer sequences were listed in Table S1.

siRNA-Mediated Gene Silencing

Scrambled siRNA control and gene-targeting siRNAs were transfected into macrophages or Kupffer cells using Lipofectamine RNAiMAX (Life Technologies) at 50 nM of siRNA in 24-well plates following the manufacturer's instructions. Briefly, the cells were incubated for 18 h with 0.5 ml of culture medium containing 1.5 μl Lipofectamine RNAiMAX per 2 X 10^5 cells and 50 nM siRNA. Cells were then incubated in complete media and experiments were conducted three days later.

Analyses of Blood Glucose and Plasma Lipids and Liver Lipids

Fasting blood glucose was measured using a glucose meter (One Touch Ultra, Life- scan) in mice that were fasted for 4-5 h, with free access to water. Total plasma triglyceride and cholesterol were assayed using commercially available kits from Wako. For liver cholesterol and triglyceride, the same kits were used on liver tissue that was homogenized in water. The suspensions were centrifuged, and the lipids in supernates were assayed with a plate reader.

QUANTIFICATION AND STATISTICAL ANALYSIS

All results are presented as mean ± SEM. Statistical significance was determined using GraphPad Prism software. P values were calculated using the Student's t-test for normally distributed data and the Mann-Whitney rank sum test for non-normally distributed data. One-way ANOVA with Bonferroni post-test was used to analyze multiple groups with only one variable tested. Two-way ANOVA with Bonferroni post-test was used to analyze more than two groups with multiple variables tested.

DATA AND CODE AVAILABILITY

This study did not generate any unique datasets or code.

Cell Metabolism, Volume *31*

Supplemental Information

Macrophage MerTK Promotes Liver Fibrosis in Nonalcoholic Steatohepatitis

Bishuang Cai, Paola Dongiovanni, Kathleen E. Corey, Xiaobo Wang, Igor O. Shmarakov, Ze Zheng, Canan Kasikara, Viralkumar Davra, Marica Meroni, Raymond T. Chung, Carla V. Rothlin, Robert F. Schwabe, William S. Blaner, Raymond B. Birge, Luca Valenti, and Ira Tabas

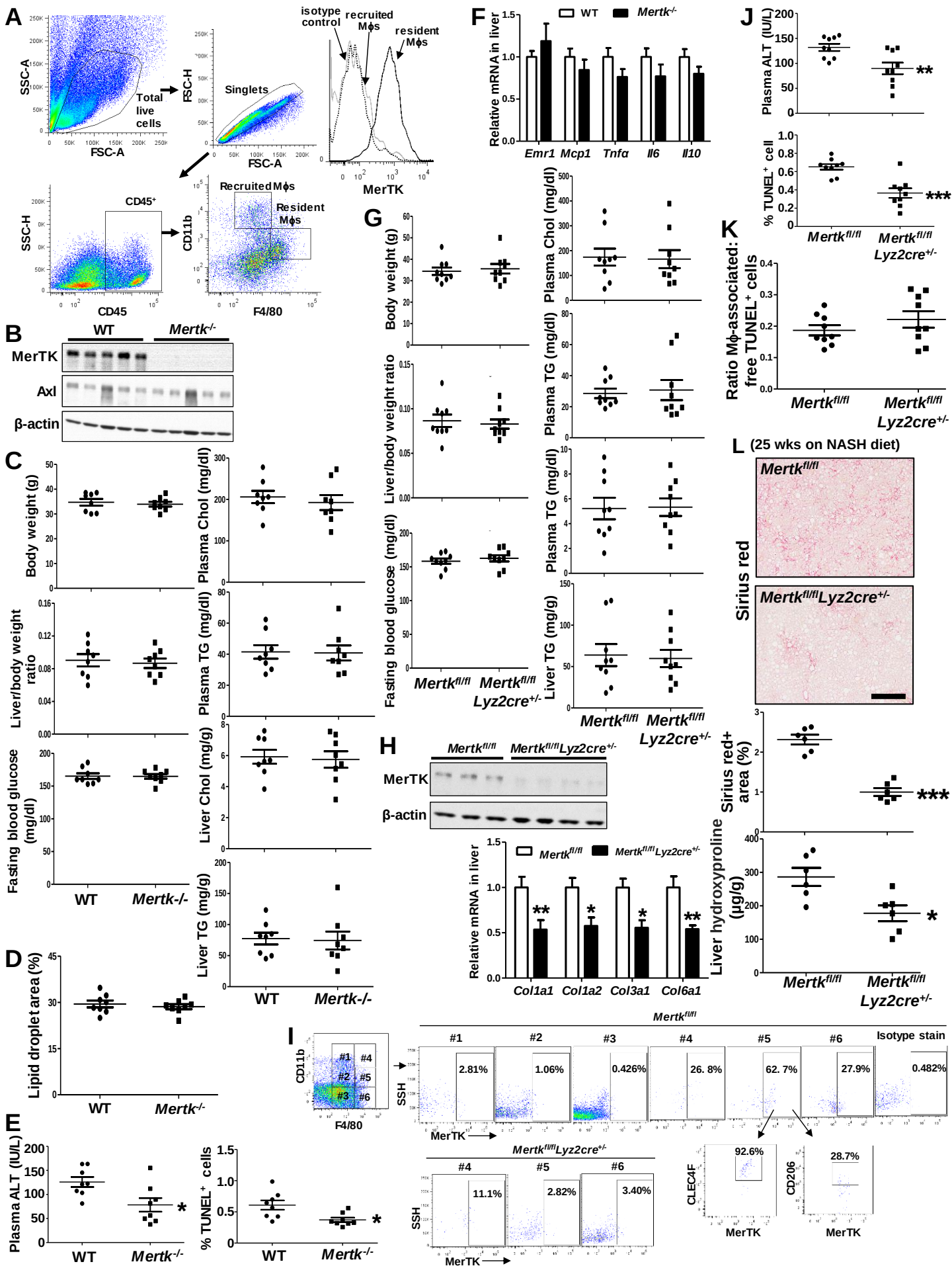
A
SSC-A
FSC-A
Total live cells
FSC-H
Singlets
isotype control
recruited Mϕs
resident Mϕs
MerTK
CD45+
CD45
SSC-H
Recruited Mϕs
Resident Mϕs
CD11b
F4/80
B
WT
Mertk-/-
MerTK
Axl
β-actin
C
Body weight (g)
Plasma Chol (mg/dl)
Liver/body weight ratio
Plasma TG (mg/dl)
Fasting blood glucose (mg/dl)
Liver Chol (mg/g)
Liver TG (mg/g)
WT
Mertk-/-
D
Lipid droplet area (%)
WT
Mertk-/-
E
Plasma ALT (IU/L)
% TUNEL+ cells
WT
Mertk-/-
F
WT
Mertk-/-
Relative mRNA in liver
Emr1
Mcp1
Tnfα
Il6
Il10
G
Body weight (g)
Plasma Chol (mg/dl)
Liver/body weight ratio
Plasma TG (mg/dl)
Fasting blood glucose (mg/dl)
Plasma TG (mg/dl)
Liver TG (mg/g)
Mertkfl/fl
Mertkfl/fl Lyz2cre+/-
H
Mertkfl/fl
Mertkfl/fl Lyz2cre+/-
MerTK
β-actin
Relative mRNA in liver
Col1a1
Col1a2
Col3a1
Col6a1
I
CD11b
F4/80
#1
#2
#3
#4
#5
#6
Mertkfl/fl
Isotype stain
SSH
MerTK
2.81%
1.06%
0.426%
26. 8%
62. 7%
27.9%
0.482%
Mertkfl/fl Lyz2cre+/-
11.1%
2.82%
3.40%
CLEC4F
CD206
92.6%
28.7%
J
Plasma ALT (IU/L)
% TUNEL+ cell
Mertkfl/fl
Mertkfl/fl Lyz2cre+/-
K
Ratio Mϕ-associated: free TUNEL+ cells
Mertkfl/fl
Mertkfl/fl Lyz2cre+/-
L
(25 wks on NASH diet)
Mertkfl/fl
Mertkfl/fl Lyz2cre+/-
Sirius red
Sirius red+ area (%)
Liver hydroxyproline (μg/g)
Mertkfl/fl
Mertkfl/fl Lyz2cre+/-

Figure S1 (Related to Figure 1). Additional Systemic and Liver Data for NASH Diet-Fed WT, *Mertk*$^{-/-}$, and *Mertk*$^{fl/fl}$*Lyz2cre*$^{+/-}$ Mice

(A) Flow cytometric analysis of cell-surface MerTK expression on resident (F4/80^{high} CD11b^{low}) and recruited (F4/80^{low} CD11b^{high}) macrophages in NASH liver.

(B-F) *Mertk*$^{-/-}$ and littermate control mice were fed the NASH diet for 16 weeks.

(B) Liver MerTK and Axl were detected by immunoblot of liver extracts.

(C) Body weight, liver/body weight ratio, fasting blood glucose, plasma cholesterol (Chol), plasma triglyceride (TG), liver cholesterol, and liver triglyceride were measured.

(D) Lipid droplet area in H&E-stained liver sections was quantified with Image J.

(E) Plasma ALT and percent TUNEL^{+} cells in the liver were assayed.

(F) The mRNAs for *Emr1*, *Mcp1, Tnfα1*, *Il6*, and *Il10* in NASH livers were assayed by qPCR.

For panels B-F, n = 8 mice per group.

(G-K) *Mertk*$^{fl/fl}$*Lyz2cre*$^{+/-}$ and control *Mertk*$^{fl/fl}$ mice were fed the NASH diet for 16 weeks.

(G) Body weight, liver/body weight ratio, fasting blood glucose, plasma cholesterol (Chol), plasma triglyceride (TG), liver cholesterol, and liver triglyceride were measured.

(H) Liver MerTK protein was assayed by immunoblot.

(I) Flow cytometric analysis of MerTK, CLEC4F, and CD206 on different CD11b- and F4/80-expressing macrophage populations isolated from *Mertk*$^{fl/fl}$ and *Mertk*$^{fl/fl}$*Lyz2cre*$^{+/-}$ NASH livers.

(J) Plasma ALT and percent TUNEL^{+} cells in the liver were assayed.

(K) The ratio of macrophage-associated to free TUNEL^{+} cells in liver was quantified.

For panels G-K, n = 9 mice per group.

(L) *Mertk*$^{fl/fl}$*Lyz2cre*$^{+/-}$ and control *Mertk*$^{fl/fl}$ mice were fed the NASH diet for 25 weeks. Liver fibrosis was detected by Sirius red staining (bar, 200 mm) and quantified as percent Sirius red^{+} area by Image J. Liver collagen gene expression was detected by qPCR, and liver hydroxyproline content was quantified using a colorimetric assay, For all data, n = 6 mice per group.

Data are presented as mean ± SEM. *p < 0.05, **p < 0.01, ***p < 0.001.

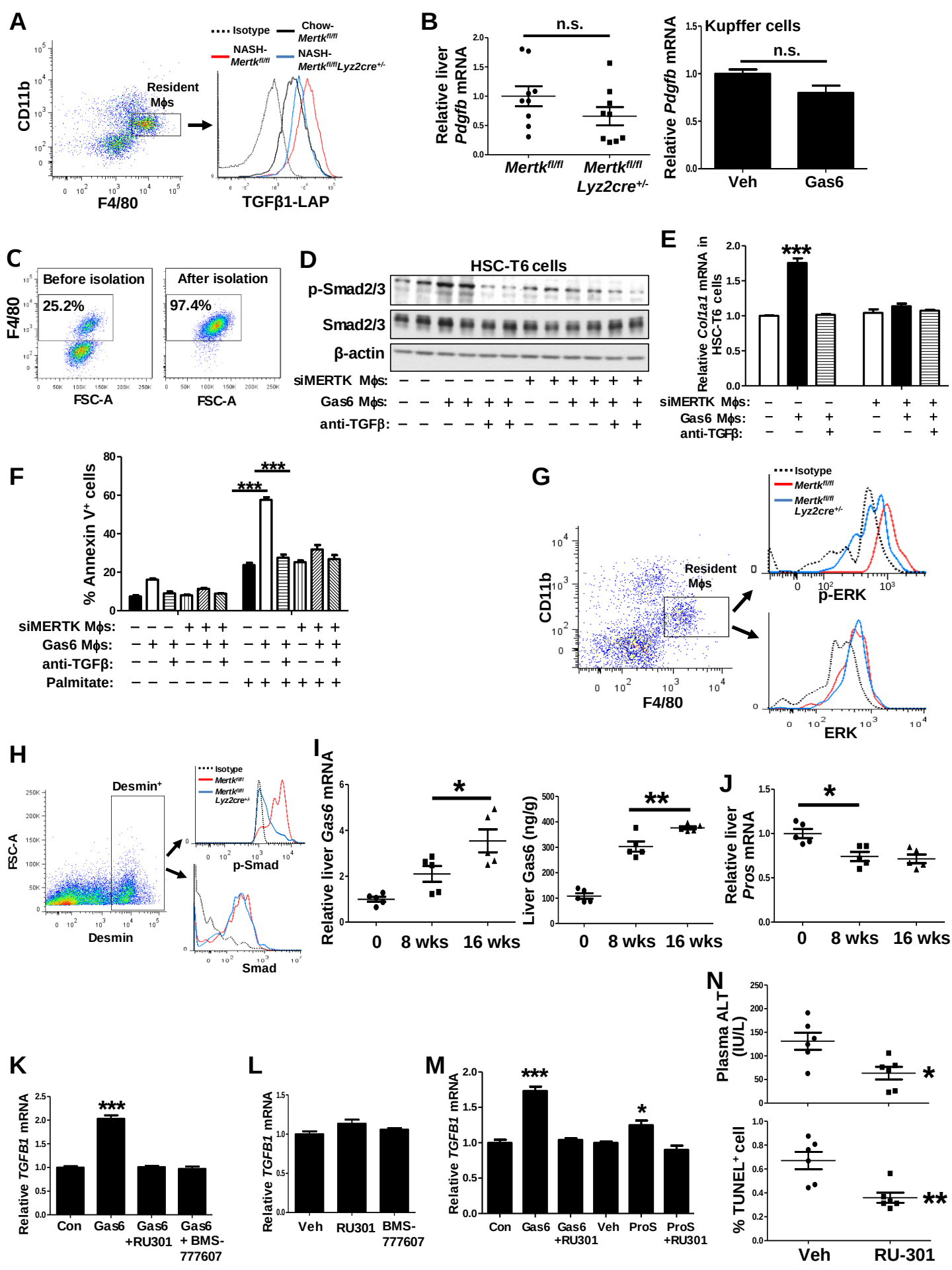
A
Isotype
Chow-Mertk fl/fl
NASH-Mertk fl/fl
NASH-Mertk fl/fl Lyz2cre +/-
CD11b
Resident Mϕs
F4/80
TGFβ1-LAP
B
n.s.
Relative liver Pdgfb mRNA
Mertk fl/fl
Mertk fl/fl Lyz2cre +/-
Kupffer cells
n.s.
Relative Pdgfb mRNA
Veh
Gas6
C
Before isolation
After isolation
25.2%
97.4%
F4/80
FSC-A
D
HSC-T6 cells
p-Smad2/3
Smad2/3
β-actin
siMERTK Mϕs:
Gas6 Mϕs:
anti-TGFβ:
E
***
Relative Col1a1 mRNA in HSC-T6 cells
siMERTK Mϕs:
Gas6 Mϕs:
anti-TGFβ:
F
***
***
% Annexin V+ cells
siMERTK Mϕs:
Gas6 Mϕs:
anti-TGFβ:
Palmitate:
G
Isotype
Mertk fl/fl
Mertk fl/fl Lyz2cre +/-
CD11b
Resident Mϕs
F4/80
p-ERK
ERK
H
Desmin+
FSC-A
Desmin
Isotype
Mertk fl/fl
Mertk fl/fl Lyz2cre +/-
p-Smad
Smad
I
*
**
Relative liver Gas6 mRNA
Liver Gas6 (ng/g)
0
8 wks
16 wks
J
*
Relative liver Pros mRNA
0
8 wks
16 wks
K
***
Relative TGFB1 mRNA
Con
Gas6
Gas6 +RU301
Gas6 + BMS-777607
L
Relative TGFB1 mRNA
Veh
RU301
BMS-777607
M
***
*
Relative TGFB1 mRNA
Con
Gas6
Gas6 +RU301
Veh
ProS
ProS +RU301
N
Plasma ALT (IU/L)
*
% TUNEL+ cell
**
Veh
RU-301

Figure S2 (Related to Figure 2). The Purity of Kupffer Cells and the Effect of MerTK Activation on *Tgfb1* mRNA

(A) Flow cytometry plot related to Figure 2A.

(B) Left, *Mertk*$^{fl/fl}$*Lyz2cre*$^{+/-}$ and control *Mertk*$^{fl/fl}$ mice were fed the NASH diet for 16 weeks. Liver *Pdgfb* mRNA was assayed by qPCR (n = 9 mice). Right, Mouse Kupffer cells were incubated for 16 h with 100 nM Gas6 and assayed for *Pdgfb* mRNA by qPCR (n = 3 plates of macrophages per group).

(C) Flow cytometric analysis of F4/80^{+} Kupffer cells before and after isolation.

(D-E) Similar to the co-culture experiment in Figure 2D, but HSC-T6 cells were used instead of primary HSCs.

(F) Similar to the co-culture experiment in Figure 2D, primary hepatocytes that had been treated with 200 μm palmitate were incubated for 24 h with the indicated macrophage conditioned media. The percentage of Annexin V^{+} hepatocytes was quantified by fluorescence microscopy (n = 4-7 plates of hepatocytes per group).

(G-H) Flow cytometry plots related to Figures 2G-H.

(I-J) Mice were fed chow diet for 16 weeks, chow diet for 8 weeks and then NASH diet for an additional 8 weeks, or NASH diet for 16 weeks. Liver extracts were assayed for *Gas6* and *Pros* mRNAs by qPCR and for Gas6 protein by ELISA (n = 5 mice per group).

(K-M) Human macrophages were treated with 100 nM Gas6 or 200 nM protein S (ProS) in the absence or presence of 5 μm RU-301 or 300 nm BMS777607. *Tgfb1* mRNA was assayed by qPCR (n = 3 plates of macrophages per condition).

(N) Plasma ALT and percent TUNEL^{+} cells in the livers of Veh- or RU-301-treated mice in Figure 2I were assayed (n = 6 mice per group).

Data are presented as mean ± SEM. *p < 0.05, **p < 0.01, ***p < 0.001, n.s, no significance.

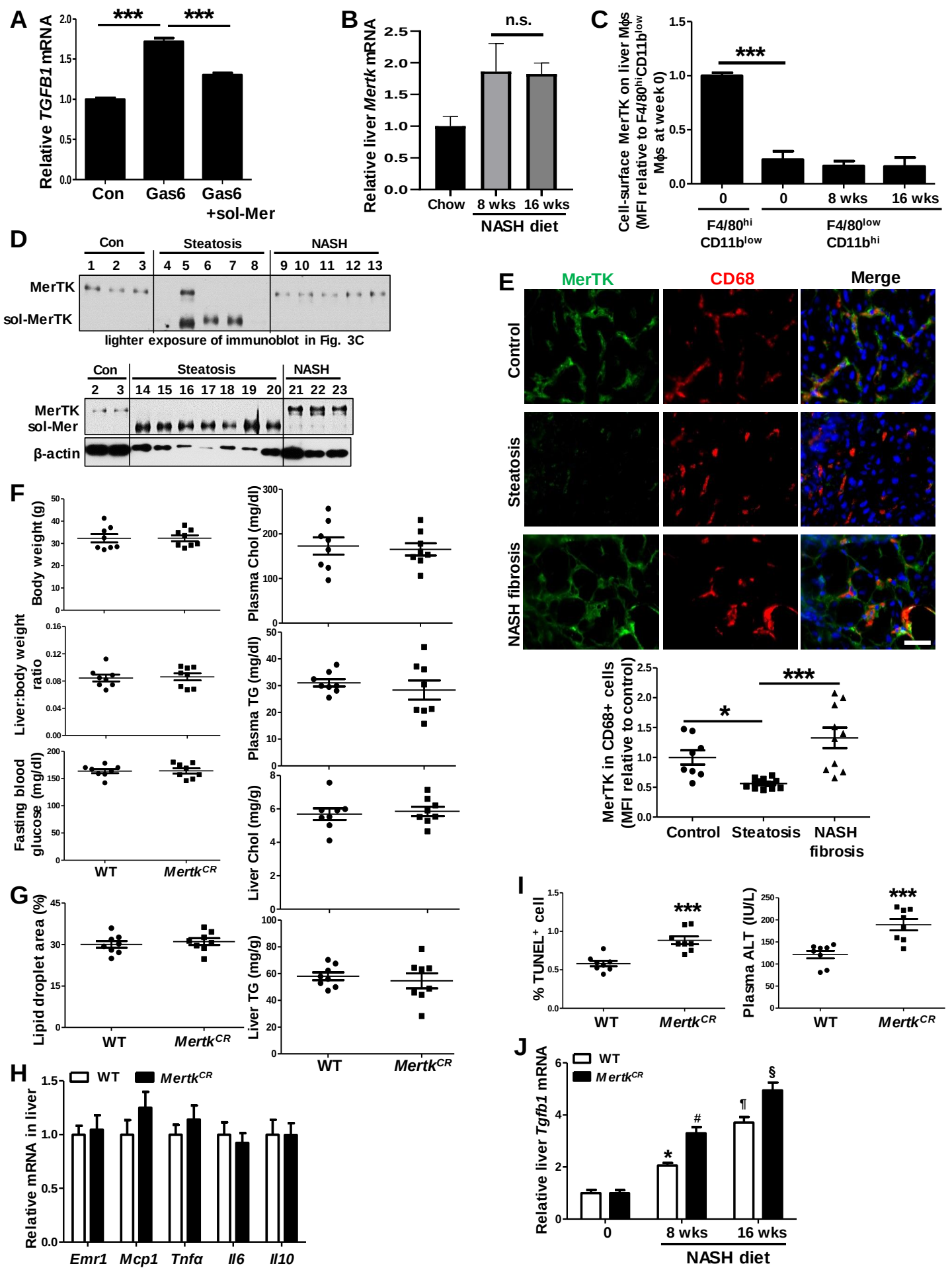
A
Relative TGFB1 mRNA
***
***
Con
Gas6
Gas6 +sol-Mer
B
Relative liver Mertk mRNA
n.s.
Chow
8 wks
16 wks
NASH diet
C
Cell-surface MerTK on liver Mϕs (MFI relative to F4/80hiCD11blow Mϕs at week 0)
***
0
0
8 wks
16 wks
F4/80hi CD11blow
F4/80low CD11bhi
D
Con
Steatosis
NASH
1 2 3 4 5 6 7 8 9 10 11 12 13
MerTK
sol-MerTK
lighter exposure of immunoblot in Fig. 3C
Con
Steatosis
NASH
2 3 14 15 16 17 18 19 20 21 22 23
MerTK
sol-Mer
β-actin
E
MerTK
CD68
Merge
Control
Steatosis
NASH fibrosis
MerTK in CD68+ cells (MFI relative to control)
*
***
Control
Steatosis
NASH fibrosis
F
Body weight (g)
Liver:body weight ratio
Fasting blood glucose (mg/dl)
Plasma Chol (mg/dl)
Plasma TG (mg/dl)
Liver Chol (mg/g)
Liver TG (mg/g)
WT
MertkCR
G
Lipid droplet area (%)
WT
MertkCR
I
% TUNEL+ cell
***
Plasma ALT (IU/L)
***
WT
MertkCR
H
WT
MertkCR
Relative mRNA in liver
Emr1
Mcp1
Tnfα
Il6
Il10
J
WT
MertkCR
Relative liver Tgfb1 mRNA
*
#
¶
§
0
8 wks
16 wks
NASH diet

Figure S3 (Related to Figure 3). MerTK Cleavage and Macrophage MerTK Expression in Human Liver, and Additional Systemic and Liver Data for NASH Diet-Fed WT and *Mertk*^{CR} Mice.

(A) Human macrophages were treated with conditioned media containing Gas6 in the absence or presence of 10 μM recombinant Mer-FC (sol-Mer) for 16 h and then assayed for *TGFB1* mRNA (n = 3 plates of macrophages per group).

(B) Mice were fed chow diet for 16 weeks, chow diet for 8 weeks and then NASH diet for an additional 8 weeks, or NASH diet for 16 weeks. Liver extracts were assayed for *Mertk* mRNA by qPCR (n = 5 mice per group).

(C) F4/80^{hi}CD11b^{low} macrophages from normal liver and F4/80^{low}CD11b^{hi} macrophages from the livers of mice on the NASH diet for 0, 8, or 16 weeks were assayed for cell-surface MerTK by flow cytometry. The data show MFI relative to the value for F4/80^{hi}CD11b^{low} macrophages from normal liver (n = 5 mice per group).

(D) Top panel: a lighter exposure of the immunoblot of human liver extracts from Figure 3C; Bottom panel: MerTK and sol-Mer were assayed by immunoblot in extracts of an additional cohort of human livers. Pathology data are shown in Table S2.

(E) Control, steatotic, and NASH human liver sections were immunostained for CD68 and MerTK under non-permeabilizing conditions. Cell-surface MerTK in CD68^{+} cells was quantified by fluorescence microscopy (n = 8-11 subjects per group); bar, 500 μm.

(F-I) WT and *Mertk*^{CR} mice were fed the NASH diet for 16 weeks.

(F) Body weight, liver/body weight ratio, fasting blood glucose, plasma cholesterol (Chol), plasma triglyceride (TG), liver cholesterol, and liver triglyceride were measured.

(G) Lipid droplet area in H&E-stained sections was quantified with Image J.

(H) The mRNAs for *Emr1*, *Mcp1, Tnfα1*, *Il6*, and *Il10* livers were assayed by qPCR.

(I) Plasma ALT and TUNEL^{+} liver cells were assayed.

For panels F-I, n = 8 mice per group. Data for A-I are presented as mean ± SEM. *p < 0.05, **p < 0.01, ***p < 0.001, n.s, no significance.

(J) *Tgfb1* mRNA in the livers of WT and *Mertk*^{CR} mice on chow diet or on the NASH diet for 8 or 16 weeks was assayed by qPCR. By two-way ANOVA, bars with different symbols were statistically different from each other at p < 0.001 for all comparisons except 8 wks versus 0 wks within the WT cohort, which was p = 0.003 (n = 5 mice per group).

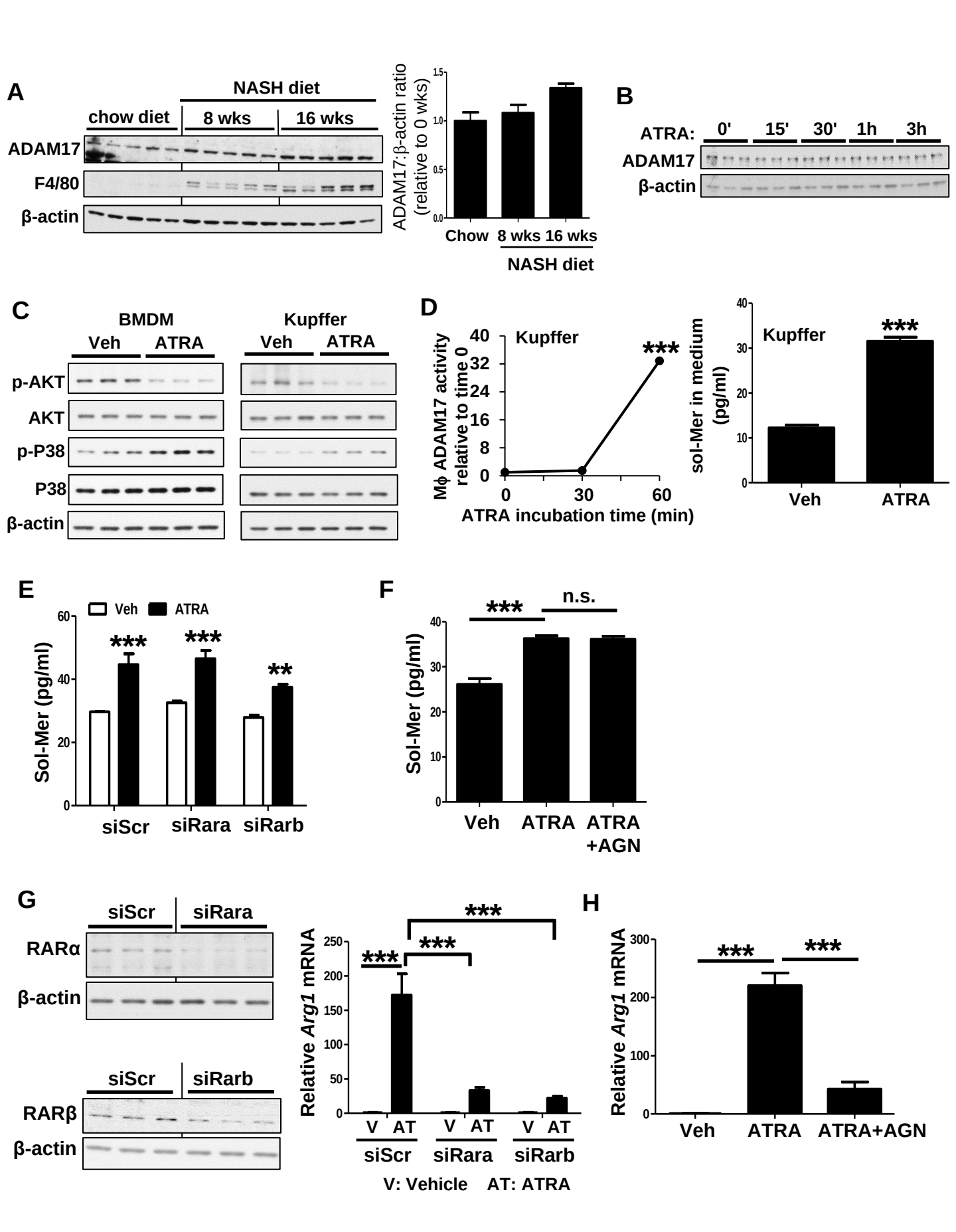
A
NASH diet
chow diet
8 wks
16 wks
ADAM17
F4/80
β-actin
ADAM17:β-actin ratio (relative to 0 wks)
Chow
8 wks 16 wks
NASH diet
B
ATRA:
0'
15'
30'
1h
3h
ADAM17
β-actin
C
BMDM
Kupffer
Veh
ATRA
p-AKT
AKT
p-P38
P38
β-actin
D
Kupffer
Mϕ ADAM17 activity relative to time 0
ATRA incubation time (min)
sol-Mer in medium (pg/ml)
Veh
ATRA
E
Veh
ATRA
Sol-Mer (pg/ml)
siScr
siRara
siRarb
F
n.s.
Sol-Mer (pg/ml)
Veh
ATRA
ATRA +AGN
G
siScr
siRara
RARα
β-actin
siScr
siRarb
RARβ
β-actin
Relative Arg1 mRNA
V
AT
siScr
siRara
siRarb
V: Vehicle AT: ATRA
H
Relative Arg1 mRNA
Veh
ATRA
ATRA+AGN

Figure S4 (Related to Figure 4). ADAM17 proteins in NASH livers and in ATRA-treated macrophages, the effect of RAR on ATRA-induced MerTK cleavage

(A) ADAM17 and F4/80 in the livers of chow-fed and NASH diet-fed mice was detected by immunoblot. The intensity ratio of ADAM17 to β-actin was quantified by Image J.

(B) BMDMs were treated with 10 μm ATRA as in Figure 4B, and ADAM17 was assayed by immunoblot.

(C) BMDMs or Kupffer cells were treated with 10 μm ATRA for 1 h as in Figure 4C. Cell lysates were immunoblotted for p-P38, P38, p-AKT, and AKT.

(D) Left panel: Kupffer cells were incubated in DMEM media containing 3% FBS for 4 h and then treated with 10 μM ATRA for the indicated times. ADAM17 activity in cell lysates was assayed at the indicated time points. Right panel: ~ 0.3 million Kupffer cells were treated with 10 μm ATRA for 3 h as in Figure 4D, and then sol-Mer in the culture medium was assayed by ELISA (n = 3 plates of cells per condition).

(E) BMDMs were treated with siScr, siRara, or siRarb for 72 h, then with 10 μm ATRA or vehicle control (Veh) for 3 h, followed by assay of sol-Mer by ELISA in the culture medium.

(F) BMDMs were treated with 10 μm RAR antagonist AGN193109 for 10 min. The cells were then treated with 10 μm ATRA or vehicle control (Veh) for 3 h, followed by assay of sol-Mer by ELISA in the culture medium.

(G) BMDMs were treated with siScr, siRara, or siRarb for 72 h. The cells were lysed for immunoblot analysis of RARα and RARβ or treated with 10 μm ATRA (AT) or vehicle control (V, Veh) for 16 h, followed by *Arg1* mRNA measurement.

(H) BMDMs were treated with 10 μm RAR antagonist AGN193109 for 10 min. The cells were then treated with 10 μm ATRA or vehicle control (Veh) for 16 h, followed by *Arg1* mRNA measurement.

For panels D-H, n = 3 plates of macrophages per condition.

Data are presented as mean ± SEM. $^{**}p < 0.01$, $^{***}p < 0.001$; n.s, no significance.

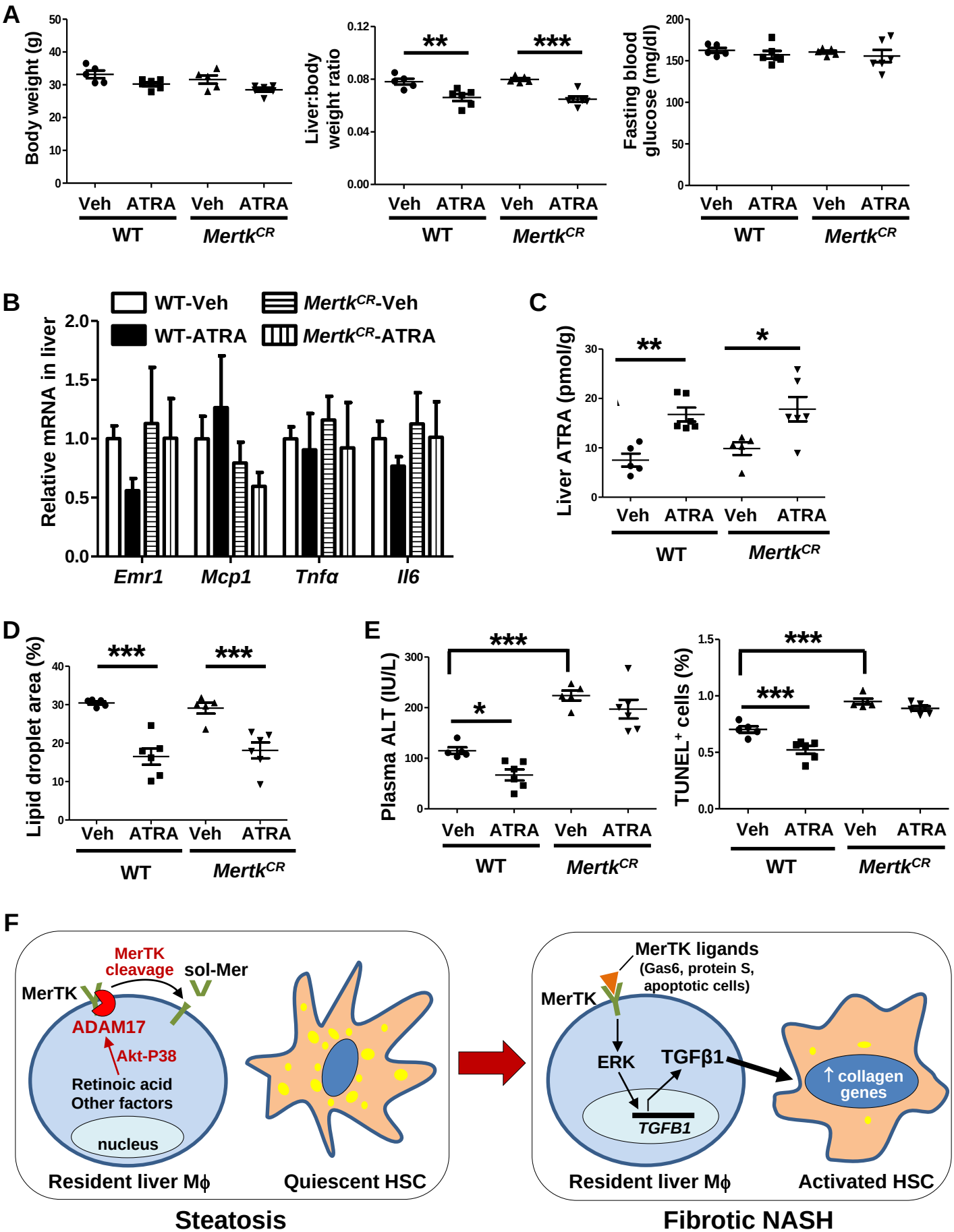
A
Body weight (g)
Liver:body weight ratio
Fasting blood glucose (mg/dl)
Veh ATRA Veh ATRA
WT
Mertk^CR
B
WT-Veh
WT-ATRA
Mertk^CR-Veh
Mertk^CR-ATRA
Relative mRNA in liver
Emr1
Mcp1
Tnfα
Il6
C
Liver ATRA (pmol/g)
D
Lipid droplet area (%)
E
Plasma ALT (IU/L)
TUNEL+ cells (%)
F
MerTK
MerTK cleavage
sol-Mer
ADAM17
Akt-P38
Retinoic acid
Other factors
nucleus
Resident liver Mϕ
Quiescent HSC
Steatosis
MerTK ligands
(Gas6, protein S,
apoptotic cells)
ERK
TGFβ1
TGFB1
↑ collagen genes
Activated HSC
Fibrotic NASH

Figure S5 (Related to Figure 5). Metabolic Parameters, Liver Inflammatory Gene Expression, Plasma ALT, and TUNEL$^+$ Liver Cells in ATRA-Treated WT and *Mertk^{CR}* Mice.

(A-E) WT and *Mertk^{CR}* mice were fed the NASH diet for 16 weeks. During the last 8 weeks, the mice were injected i.p. with 15 µg/g body weight ATRA or vehicle control three times a week.

(A) Body weight, liver/body weight ratio, and fasting blood glucose were measured

(B) The mRNAs for *Emr1*, *Mcp1, Tnfα1*, and *Il6* in NASH livers were assayed by qPCR.

(C) Liver ATRA was determined by LC-MS/MS.

(D) Lipid droplet area in H&E-stained sections was quantified with Image J.

(E) Plasma ALT and TUNEL$^+$ liver cells were assayed.

For all panels, n = 5-6 mice per group.

(F) Summary scheme of MerTK-macrophage HSC crosstalk pathway in fibrotic NASH. In steatosis, MerTK cleavage in resident macrophages suppresses MerTK signaling, and HSCs, which store retinoids in cytoplasmic lipid droplets, remain quiescent. In this setting, a retinoic acid-P38-ADAM17 activation pathway in macrophages contributes to MerTK cleavage. During progression to fibrotic NASH, MerTK signaling is restored by suppression of MerTK cleavage. This signaling leads to ERK1/2 activation and *TGFB1* induction, and the resulting increase and secretion of TGFβ1 from these macrophages activates HSCs into a pro-fibrotic phenotype.

Data are presented as mean ± SEM. *p < 0.05, **p < 0.01, ***p < 0.001.

Table S1 (Related to all figures). Primers used for QPCR.

Primers	Sequences
Hprt F (mouse)	TCAGTCAACGGGGGACATAAA
Hprt R (mouse)	GGGGCTGTACTGCTTAACCAG
Tgfb1 F (mouse)	CTCCCGTGGCTTCTAGTGC
Tgfb1 R (mouse)	GCCTTAGTTTGGACAGGATCTG
Tgfb2 F (mouse)	CTTCGACGTGACAGACGCT
Tgfb2 R (mouse)	GCAGGGGCAGTGTAAACTTATT
Tgfb3 F (mouse)	CCTGGCCCTGCTGAACTTG
Tgfb3 R (mouse)	TTGATGTGGCCGAAGTCCAAC
Col1a1 F (mouse)	GCTCCTCTTAGGGGCCACT
Col1a1 R (mouse)	CCACGTCTCACCATTGGGG
Col1a2 F (mouse)	GTAACTTCGTGCCTAGCAACA
Col1a2 R (mouse)	CCTTTGTCAGAATACTGAGCAGC
Col3a1 F (mouse)	CTGTAACATGGAAACTGGGGAAA
Col3a1 R (mouse)	CCATAGCTGAACTGAAAACCACC
Col6a1 F (mouse)	GATGAGGGTGAAGTGGGAGA
Col6a1 R (mouse)	CAGCACGAAGAGGATGTCAA
F4/80 (*Adgre1*) F (mouse)	ACCACAATACCTACATGCACC
F4/80 (*Adgre1*) R (mouse)	AAGCAGGCGAGGAAAAGATAG
Tnfa F (mouse)	CTTCTGTCTACTGAACTTCGGG
Tnfa R (mouse)	CAGGCTTGTCACTCGAATTTTG
Mcp1 F (mouse)	TTAAAAACCTGGATCGGAACCAA
Mcp1 R (mouse)	GCATTAGCTTCAGATTTACGGGT
Il6 F (mouse)	TAGTCCTTCCTACCCCAATTTCC
Il6 R (mouse)	TTGGTCCTTAGCCACTCCTTC
Il10 F (mouse)	GCATGGCCCAGAAATCAAGG
Il10 R (mouse)	AGGGGAGAAATCGATGACAGC
Pdgfb F (mouse)	CATCCGCTCCTTTGATGATCTT
Pdgfb R (mouse)	GTGCTCGGGTCATGTTCAAGT
Hprt F (human)	CCTGGCGTCGTGATTAGTGAT
Hprt R (human)	AGACGTTCAGTCCTGTCCATAA
Tgfb1 F (human)	GGCCAGATCCTGTCCAAGC
Tgfb1 R (human)	GTGGGTTTCCACCATTAGCAC
Gapdh F (rat)	CCATTCTTCCACCTTTGATGCT
Gapdh R (rat)	TGTTGCTGTAGCCATATTCATTGT
Col1a1 F (rat)	ATCAGCCCAAACCCCAAGGAGA
Col1a1 R (rat)	CGCAGGAAGGTCAGCTGGATAG

Hprt, hypoxanthine guanine phosphoribosyl transferase; *Tgfb1*, transforming growth factor, beta 1; *Tgfb2*, transforming growth factor, beta 2; *Tgfb3*, transforming growth factor, beta 3; *Col1a1*, collagen type I alpha 1; *Col1a2*, collagen type I alpha 2; *Col3a1*, collagen, type III alpha 1; *Col6a1*, collagen type IX alpha 1; *F4/80* (*Adgre1*), adhesion G protein-coupled receptor E1; *Tnfa*, tumor necrosis factor-α ; *Mcp1*, monocyte chemoattractant protein-1; *Il6*, interleukin 6; *Il10*, interleukin 10; *Pdgfb*, platelet derived growth factor, beta; *Gapdh*, glyceraldehyde-3-phosphate dehydrogenase.

Table S2 (Related to Figures 3C and S3D). Pathology scoring of human liver samples.

Subject #	Steatosis	Necroinflammation	Fibrosis	Ballooning	NAS
1	0	0	0	0	0
2	0	0	0	0	0
3	0	0	0	0	0
4	1	0	0	0	1
5	1	0	0	0	1
6	1	0	0	0	1
7	1	0	0	0	1
8	1	0	0	0	1
9	1	1	1	0	2
10	2	1	1	0	3
11	2	1	1	0	3
12	1	1	1	0	2
13	3	1	1	1	5
14	3	1	0	0	4
15	3	1	0	0	4
16	2	1	0	1	4
17	2	1	0	0	3
18	2	1	0	0	3
19	3	2	0	0	5
20	3	1	0	1	5
21	2	1	2	0	3
22	2	1	3	0	3
23	3	1	1	1	5